2017

Numerical and Experimental Study of the Melting Process of a Phase Change Material in a Partically Filled Spherical Shell

Wen Xiong
Lehigh University

Numerical and Experimental Study of the Melting Process of a Phase Change Material in a Partially Filled Spherical Shell

by

Wen Xiong

Presented to the Graduate and Research Committee

of Lehigh University

in Candidacy for the Degree of

Master of Science

in

Mechanical Engineering

Lehigh University

(May 2017)

This thesis is accepted and approved in partial fulfillment of the requirements for the Master of Science.

_____
Date

_____
Dr. Arindam Banerjee, Thesis Advisor

_____
Dr. Gary Harlow, Chairperson of Department

ACKNOWLEDGMENTS

I would like to express my greatest appreciation to my thesis advisors, Dr. Arindam Banerjee, Dr. Sudhakar Neti, and Dr. Carlos Romero. They always answered my questions patiently and guided me in the right direction during my research work. Additionally, I would like to thank CJ Pan and all the other friends at the Energy Research Center, for teaching me how to use Fluent and for many though-provoking conversations.

I am also appreciative of my family for always believing me and encouraging me to pursue my dream and to work hard abroad. Additionally, I would like to thank my roommate Gongming Zhang for all his daily life help throughout the years. Lastly, special thanks to Dr. Carlos Romero again for his countless hours of thesis guidance and proofreading.

TABLE OF CONTENTS

LIST OF TABLES

LIST OF FIGURES

ABSTRACT

A three dimensional axisymmetric model of the heat transfer during the melting process of a phase change material (PCM) inside a spherical container was analyzed both numerically and experimentally. A study of PCM phase change is important to understand the behavior of these materials in thermal storage applications. A void space was provided within the container to consider the volumetric expansion of PCM during the melting process. The PCM's properties used in the simulations, include the melting temperature, latent and sensible specific heat, thermal conductivity, and density in the solid and liquid states, and were based on a commercially available salt hydrate, calcium chloride hexahydrate. This salt has been used mainly in latent heat-based heat storage systems. The mathematical model was solved using the "Volume of Fluid Method," and the "Enthalpy-Porosity Formulation" was employed to solve the energy equations in both the liquid and solid regions of the PCM, using the Fluent software. A detailed sensitivity investigation was performed for melting in spherical shells of 40, 60, and 80 mm in diameter, while the outer surface temperature of the container was set to 5, 10, and 15 °C above the mean melting temperature of the PCM. The simulations showed the melting process from the start of phase change to the end, and incorporated some phenomena such as convection in the liquid phase, volumetric expansion due to melting, sinking of the solid phase, and close contact melting. It was found that at a constant value of Stefan Number, increasing the Grashof Number will enhance the heat transfer rate. Additionally, the combined effect of the Grashof and Stefan Numbers at an increase of the outer surface temperature of the enclosure could also enhance the melting rate of the PCM. Finally, appropriate dimensionless variables, based on a combination of the Fourier, Grashof and Stefan Numbers, were introduced in order to obtain a generalized correlation for the liquid mass fraction and the Nusselt Number during melting of the phase change material.

CHAPTER 1: INTRODUCTION

1.1 Motivation

With the current penetration of renewable energy, such as wind and solar, into the electrical grid, there is an inevitable need to increase the dispatching ability of these power sources. Solar energy is one of the most attractive energy sources in the world. As a kind of clean renewable energy option, it is receiving a lot of attention due to the finite quantities of fossil fuels and the pollution drawback associated with them. However, large scale electricity supply using solar energy is still not fully competitive with current fossil fuel power plants. There is a range of research needs for wide-spread utilization of solar energy that includes grid connectivity, efficient solar energy collection, energy storage, etc.

There are two popular approaches to use solar energy for electricity generation: one is utilizing photovoltaic (PV) cells to convert solar radiation into electric energy directly; the other one is conversion of solar radiation into thermal energy for electric power generation, for example in a concentrating solar power (CSP) plant. It has been reported that both of these methods suffer from low capacity factors of solar energy conversions. Solar power plant capacity factors are around 18% while the capacity factors of traditional fossil fuel power plant are in the 85% range. Capacity factor is a measure of the percentage of a plant's potential energy output that is actually delivered over a period of time. One efficient way to enhance the capacity factor of CSP plants is to employ thermal energy storage (TES). TES systems would store parts of the solar energy captured during times of high solar radiation for subsequent use. Solar thermal power also has the ability to easily integrate TES without incurring into a costly conversion processes. As a result, this makes CSP plants with a TES system to become a highly attractive form of grid-scale

electricity generation. However, research is needed to develop and adapt new materials, develop modeling tools, and engineer full-scale systems for production of efficient CSP plants with TES.

1.2 Thermal Energy Storage

TES could be classified into three forms, based on the energy storage process mechanism: sensible heat storage, latent heat storage, and thermo-chemical heat storage. In sensible heat storage systems, energy is stored and released by raising or lowering the temperature of a material. The amount of energy stored depends on the heat capacity of the material and the temperature difference applied to the material. While sensible heat storage systems rely on large temperature differences, latent heat-based storage systems can store energy under nearly isothermal conditions, by utilizing the large quantity of energy required to induce a change of state within a material. In a similar way, thermochemical energy storage systems use reversible endothermic/exothermic reactions to store and release energy. To reduce the cost of a TES system, a material with a high energy storage density should be used. While thermochemical systems have the highest energy storage density of the three forms of TES systems, research in this area is still in the early stages and uncertainties in thermodynamic properties, phase change process, as well as reaction kinetics limit its usage.

The most common of sensible heat TES systems use either a large volume of a solid material, such as concrete, or a single or two-tank molten salt-based storage system [1, 2]. These systems require a large volume of material to store enough energy to efficiently operate a mid-sized plant for eight hours. For example, 28,500 tons of molten salt is required to operate the 150 MW Andasol power plant in Spain for 7.5 hours. If a latent heat based storage system was used instead, the amount of storage material could be greatly reduced, yielding a lower system cost. This would

result in a decrease in the levelized cost of electricity (LCOE) for CSP plants, making them not only cost competitive with current fossil fuel-based plants but with other means of renewable energy as well.

1.3 Phase Change Materials

A phase change material (PCM) is the main component of a latent heat-based TES system. Any material that undergoes a phase state change could potentially be used as a PCM for TES applications. Four different state or phase changes can occur: solid-solid, solid-liquid, liquid-gas, and solid-gas. During a solid-solid phase change the crystal structure of a material changes from one lattice configuration to another. While the small volumetric changes that occur during solid-solid phase changes make them ideal candidates for TES, the transitions are typically slow and have low transformation enthalpies relative to the other state changes. The state change that is typically studied for TES applications is that of solid-liquid phase change due to their relatively small volume change and moderate enthalpy change. Although, liquid-gas transitions have high transformational energies, the large volume changes that occur and the complexity of storing the gaseous medium limit their use for TES applications. The last state transformation is when a solid material directly turns into a gas, such as dry ice. Solid-gas transitions have the same drawbacks as with the use of liquid-gas transitions. Therefore the solid-liquid phase change is best suited for TES.

Whereas numerous materials exist that have melting temperatures in different temperature ranges, this alone does not make them a viable PCM for TES applications. It is required that the material also exhibit other desirable thermo-physical, kinetic, and chemical properties such as a high latent heat of fusion, small volume change, sufficient crystallization rate, and chemical

stability, all while being commercially abundant at low cost [3]. PCMs can be divided into three groups: organic, inorganic, and eutectic materials. A diagram of the classification of PCMs is shown in Fig. 1. Table 1 also presents a comparison of different PCM groups [4]. Research has been conducted into potential materials for use in latent heat based TES at temperatures below 120 °C [5-9]. This range of temperature is of great interest in supplemental cooling applications for power plants. The list of materials suitable for this temperature range includes paraffin waxes, fatty acids, and salt hydrates. Storage of thermal energy using latent heat-based on phase change material is an attractive method to store renewable thermal energy since it could enable near isothermal and high exergy storage conditions.

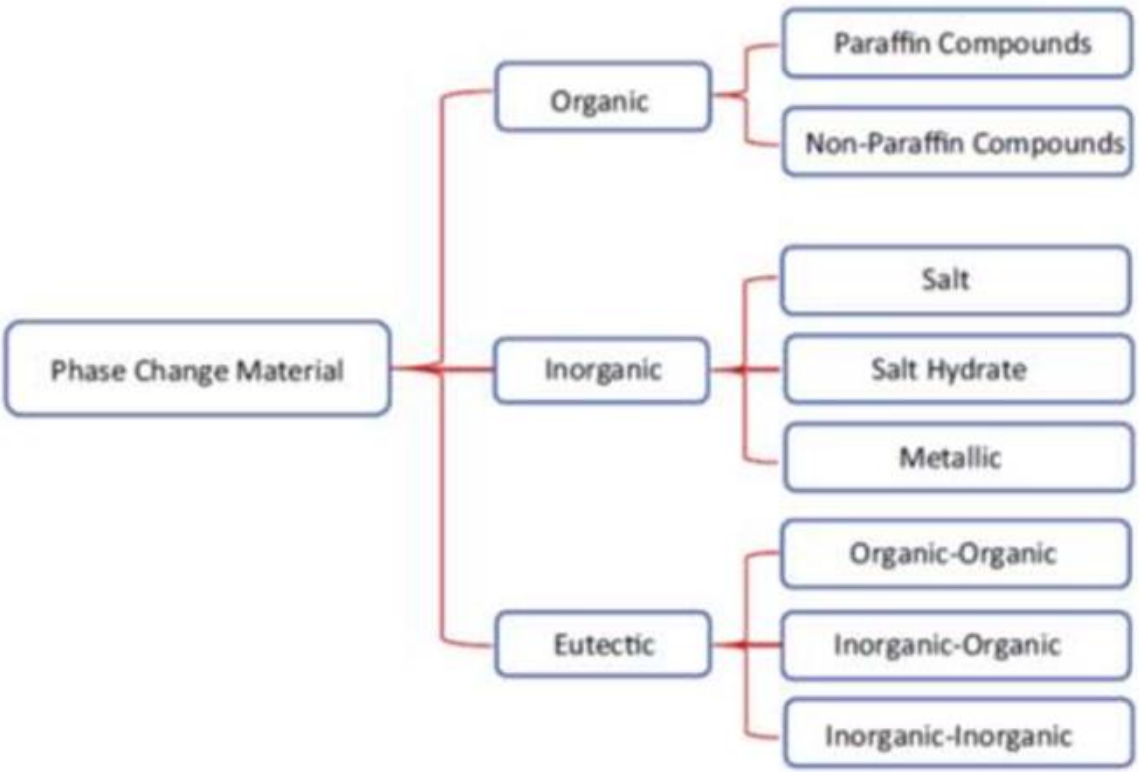

Fig. 1. Classification of Phase Change Materials in Reference 4

Table 1. Comparison of Different PCM Groups in Reference 4

Classification	Advantages	Disadvantages
Organic PCMs	Available in a large temperature range	Low volumetric latent heat storage capacity
	Low or non supercooling	Low thermal conductivity
	Chemically stable and recyclable	Relative large volume change
	Good compatibility with other materials	Flammability
Inorganic PCMs	High heat of fusion	Supercooling
	High thermal conductivity	Phase separation
	Low volume change	Lack of thermal stability
	Availability and cheapness	Corrosion
Eutectics	Sharp melting temperature	Lack of test datum of thermophysical properties
	High volumetric thermal storage density	

1.4 Definition of Problem with PCM Solid Sinking

Being solid-liquid phase change PCMs of great interest in TES, it is of capital importance to understand and study the phase change process, to the extent that it can be well characterized for its application. This includes modeling solutions that can be employed in the design of physical TES systems that induce solid-liquid phase change PCMs. One particular aspect of this phase change process is the issue of solid phase sinking in the liquid phase. This aspect is important since it involves heat transfer, thermodynamics and fluid flow processes which need to be well represented for a correct characterized melting process. The processes involved in phase change are not the same for different materials. For instance, when an enclosed cubic ice melts in water, the total volume decreases due to the fact that its density is lighter than liquid water [10]. The solid fraction floats at the surface of the melted water. A cubic shape of the solid fraction is retained for most of the melting process except towards the end when it loose its cubic shape and becomes flattened or elongated until melting is completed. On the other hand, for a phase change material whose solid state is denser than the liquid state, it is expected that the solid bulk will move vertically downward due to the gravity. The latter situation is physically shown in Fig. 2 [11],

where a constant higher temperature T_w is imposed at the bottom of a container storing the PCM for melting to begin. The motion of the solid bulk is accompanied by generation of liquid at the melting interface. Because the solid phase sinks down, the liquid is squeezed up through the narrow gap between the bottom melting surface and the bottom of the shell, flowing through the gap between the solid phase and the vertical container walls to the space above the solid. In this situation, the effect of solid sinking and appearance of "Close Contact Melting" [11, 12] is very significant. "Close Contact Melting" is used to represent a heat source and a solid are pressed against each other while the solid begins melting.

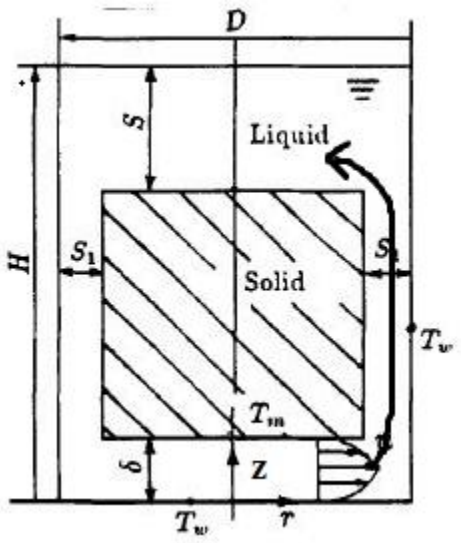

Fig. 2. Close Contact Melting Model in Reference 12

This thesis reports a study to analyze the melting process of PCMs, including solid phase sinking. As part of this study, a numerical study was undertaken that simultaneously model the conservation equations for solid PCM, liquid PCM, and air in a three dimensional axisymmetric spherical model, while allowing for PCM expansion, and convection between liquid PCM and air. This simulation model was solved using the "Volume of Fluid Method." The "Enthalpy-Porosity

Formulation" was employed to solve the energy equations in both the liquid and solid regions of the PCM. The model was solved using the Fluent software. An experiment was also set up to validate the results from the simulations. A detailed sensitivity analysis was also performed of melting in spherical shells of 40, 60, and 80 mm in diameter, with outer surface temperatures of 5, 10, and 15 °C above the mean melting temperature of the PCM. Additionally, in order to obtain generalized results, a dimensional analysis was performed and presented as a function of the Nusselt Number and melting fraction vs. the Fourier and Stefan Numbers and geometry parameters.

CHAPTER 2: LITERATURE REVIEW

In recent years, phase change materials have been attracting the attention of researchers due to their exceptional behavior, such as high storage density, chemical stability, and small temperature drop during heat recovery process. In the early 1980s, scientists began to look into the details of the melting process of PCMs in spherical and cylindrical enclosures [13-14]. A numerical analysis of PCM melting in a horizontal cylinder, performed by Nicholas and Bayazitoglu [15], was an initial attempt to consider the effect of density change between solid and liquid, while neglecting convective motion in the melt. Roy and Sengupta [16] studied PCM melting in a spherical geometry, treating the entire melting process analytically. Their analytical method is similar to that proposed by Bareiss and Beer [12] for a horizontal cylinder, but with a different approach to treat the liquid film between the solid and the wall. The process in Reference 12 was assumed to be quasi-steady, no melting was assumed at the top surface of solid PCM, and the heat transfer was assumed to occur through the liquid film only.

Based on a review of these references, modeling of the PCM melting process is a considerable challenge, there are issues to be considered associated with the non-linear behavior of the melting point, convection phenomena in the melt, volumetric expansion, motion of solid in the melt, and motion of liquid around the solid and the wall of the PCM enclosure. Due to these difficulties, the PCM phase changing process has been simplified by approximating or even neglecting some of these phenomena when an analytical solution is attempted. In the next paragraphs, description of recent reports on PCM phase change process is summarized in more detail. These literature results are also included here because they were used for model validation in this study.

Darzi and Afrouzi [17] performed a numerical study of unconstrained solidification and melting of phase change material inside a two dimensional open rectangular cavity to demonstrate that conduction heat transfer was the dominant mechanism at the initial time of the melting process. Over time, the gravity and the difference between solid and liquid density of the PCM forced the solid state PCM to sink down towards the bottom of the container and pushed up hot liquid PCM, which intensified the convection force and accelerated the melting rate. A schematic of the computational domain in reference 17 is shown in Fig. 3. The bottom surface was assumed heated at a temperature of 39°C, and the two side walls serve as vertical fins for the cavity. The properties of the PCM were based on a commercially available material, RT-27 (Rubitherm GmbH), and are displayed in Table 2. Additionally, the size of the rectangle is 42 mm x 42 mm, and the PCM fills 85% of the enclosed space. The fin thickness is 2 mm.

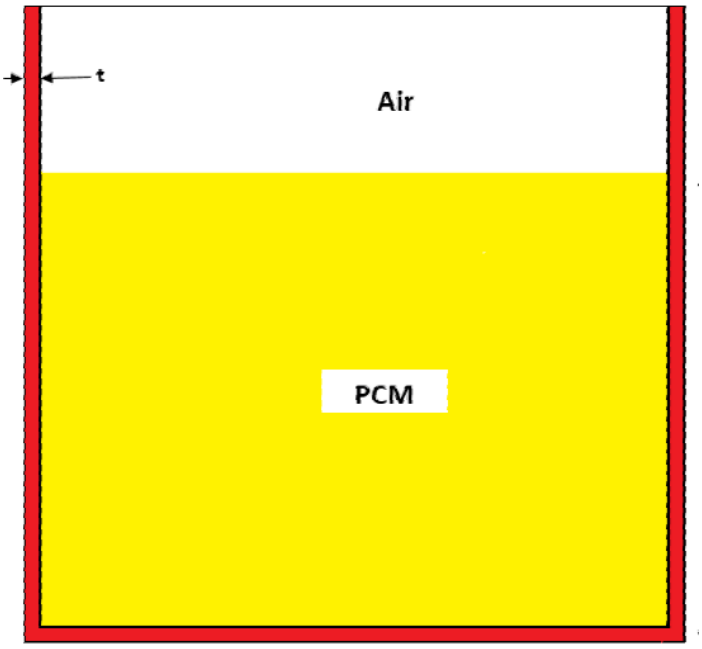

Fig. 3. Schematic of Computational Domain in Reference 17

Table 2. Thermal Properties of RT-27 in Reference 17

Melting temperature	28-30°C
Density (Solid-Liquid)	870-760 kg/ m^3
Kinematics Viscosity	3.42×10^{-3} m^2/s
Specific Heat (Solid-Liquid)	2400-1800 J/kg K
Thermal Conductivity (Solid-Liquid)	0.24-0.15 W/m K
Latent Heat of Fusion	179 kj/kg
Thermal Expansion Coefficient	0.0005 K^{-1}

Archibold and Aguilar [18] reported numerical analyses of melting in a closed spherical enclosure, which is shown in Fig. 4. A combined PCM-air system was analyzed with the air space in the upper part of the shell accounted for the volume expansion during the phase change process. This study was based on a low melting point sodium nitrate in a nickel alloy container, submerged into a water bath with a temperature of 10°C above the mean melting temperature of the sodium nitrate. The thermo-physical properties of the materials used in Reference 18 are listed in Table 3. The spherical model had an internal radium of 15 mm, and the thickness of the shell is 0.5 mm. Sodium nitrate initially occupied 85% of the enclosure volume. This model takes into account the density difference between the solid and liquid PCM, the natural convection in the molten PCM and the air, and the vertical motion of solid PCM.

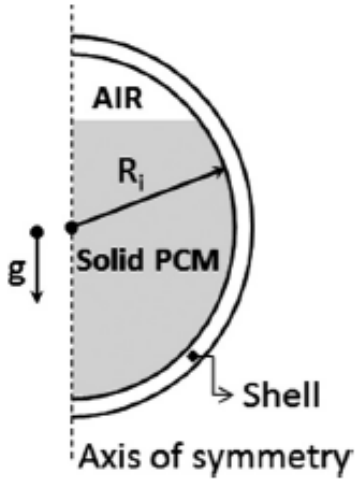

Fig. 4. Computational Domain in Reference 18

Table 3. Thermo-Physical Properties of Materials in Reference 18

Properties	Sodium Nitrate	Nickel alloy	Air
Density (kg/m^3)			Ideal gas
Solid phase	2130	8400	
Mushy zone	$259405.8-444T$		
Liquid phase	$2333.9-0.7665T$		
ρ_l (kg/m^3)	1908		
Dynamic viscosity (kg/m s)	$0.01192-1.53\times10^{-5}T$		2.92×10^{-6}
Latent heat of fusion (J/kg)	178000		
Melting temperature (°C)	306.8		
Specific heat (J/kg K)	$444.53+2.18T$	507.22	1047
Thermal expansion coef. (K^{-1})	6.6×10^{-4}		
Thermal conductivity (W/mK)	$0.3057+4.47\times10^{-4}T$	16.74	0.0454

The results of Reference 17 and 18 provided on a melt fraction plot versus time are presented in Figs. 5 and 6, respectively. The total melting time of Reference 17 and 18 are 10.8 mins and 8 mins, respectively. These results were also reproduced as parts of this study. The reproduced results were respectively compared with the original results of these two literature at the end of the next chapter for validation purposes.

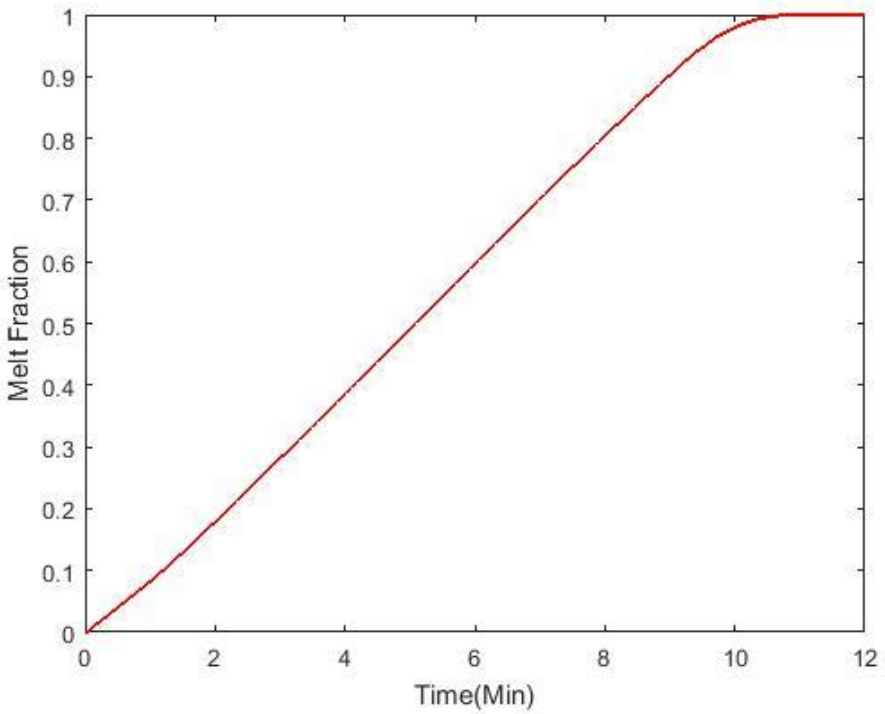

Fig. 5. Results from Reference 17

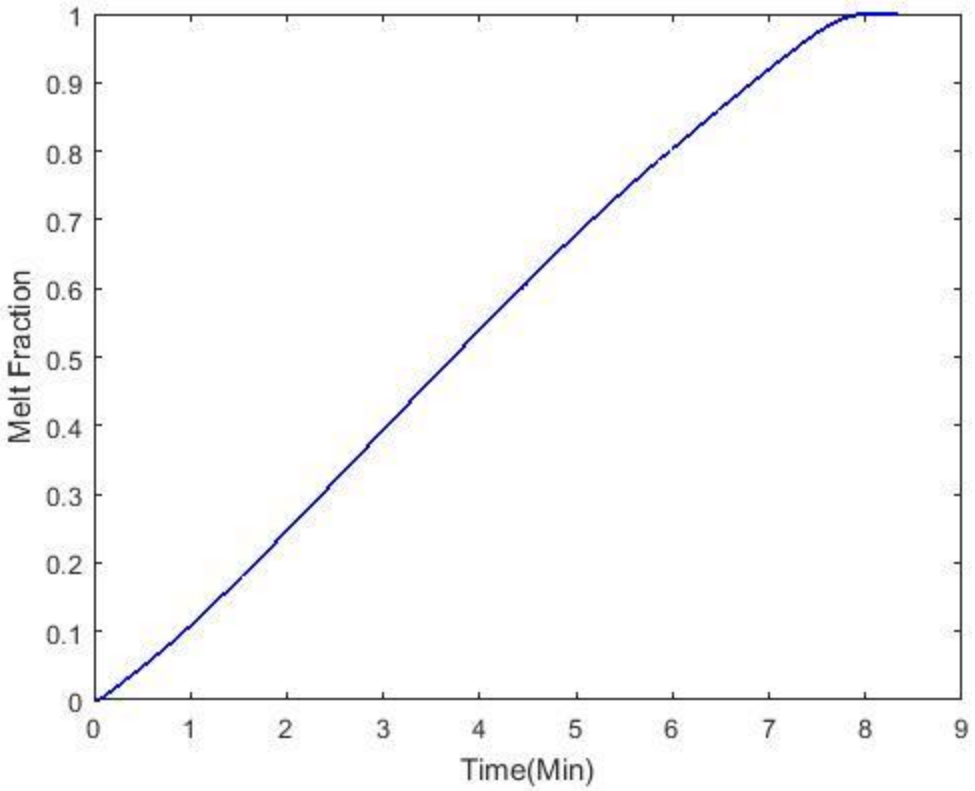

Fig. 6. Result of Reference 18

CHAPTER 3: NUMERICAL STUDY

This chapter describes the physical model used for the simulations of the PCM phase changing process, including solid sinking. The computational procedure is also describes in this chapter.

3.1 Characteristics of Phase Change Material Used in Simulations

The melting temperature and phase change enthalpy of different types of low-temperature phase change materials are shown in Fig. 7 [4]. By observing the temperature of the melting point and the enthalpy of fusion, it is not hard to find that salt hydrates and eutectics (an alloy or mixture whose melting point is lower than that of the other alloys in the mixture or mixture of the same individual components) are one type of PCM suited for latent heat storage in low- to mid-temperature applications, as the one of interest in this study.

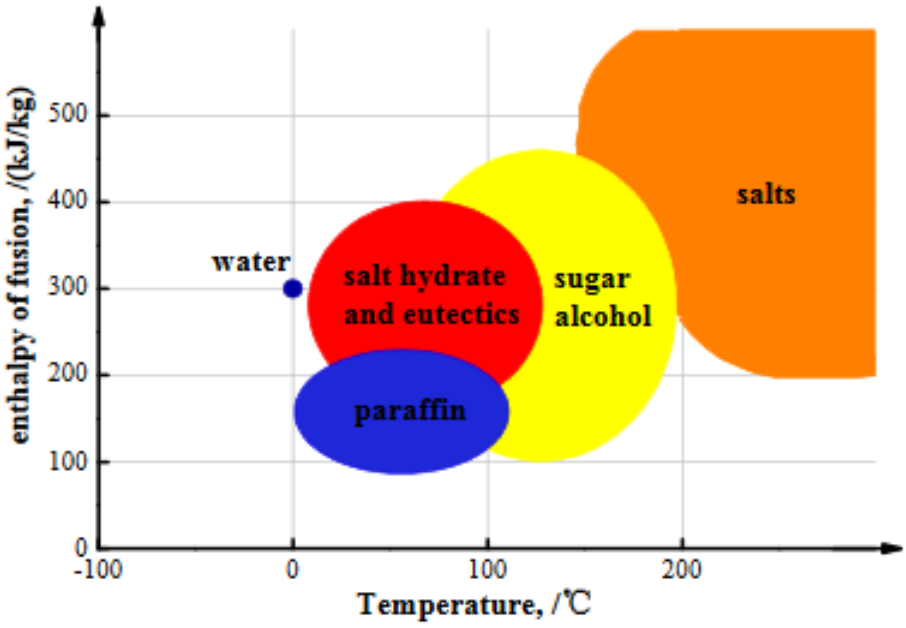

Fig. 7. Melting Temperature and Latent Heat of Different PCMs in Reference 4

One type of salt hydrates, calcium chloride hydrates, are materials with desirable thermodynamic, kinetic, and physical properties and chemical properties. These salts meet economic and availability considerations for power plant cooling applications that are of interested in CSP applications, which provided motivation on this study. Of particular interest is the 20-25°C temperature range to be used as supplemental cooling, supporting the operation of once-through condensers and cooling towers in power plant applications. They can be purchased at online stores with typical price in the $1.5 per kilogram range. Properties of calcium chloride and its hydrates are list in Table 4.

Table 4. Properties of Calcium Chloride and its Hydrates in Reference 4

Property	$CaCl_2 \cdot 6H_2O$	$CaCl_2 \cdot 4H_2O$	$CaCl_2 \cdot 2H_2O$	$CaCl_2 \cdot H_2O$	$CaCl_2$
Composition (% $CaCl_2$)	50.66	60.63	75.49	86.03	100
Molecular Weight	219.09	183.05	147.02	129	110.99
Melting Point[1] (°C) (°F)	29.9 85.8	45.3 113.5	176 349	187 369	773 1424
Boiling Point[2] (°C) (°F)	– –	– –	174 345	183 361	1935 3515
Density at 25°C (77°F), g/cm³	1.71	1.83	1.85	2.24	2.16
Heat of Fusion (cal/g) (BTU/lb)	50 90	39 70	21 38	32 58	61.5 110.6
Heat of Solution[3] in H_2O (cal/g) (to infinite dilution) (BTU/lb)	17.2 31.0	-14.2 -25.6	-72.8 -131.1	-96.8 -174.3	-176.2 -317.2
Heat of Formation[3] at 25°C (77°F), kcal/mole	-623.3	-480.3	-335.58	-265.49	-190.10
Heat of Capacity at 25°C (77°F), cal/g°C or BTU/lb°F	0.34	0.32	0.28	0.20	0.16

For this study, $CaCl_2 \cdot 6H_2O$ was selected as the target PCM due to its low melting point and high latent heat. A real salt hydrate, like $CaCl_2 \cdot 6H_2O$, does not have precisely defined temperature for its solid and liquid state during the phase changing process, and its enthalpy is a continuous function of temperature. Detail thermos-physical properties of $CaCl_2 \cdot 6H_2O$ are displayed in Table 5.

Table 5. Thermo-physical properties of $CaCl_2 \cdot 6H_2O$

Meting Temperature	29 °C
Density (Solid-liquid)	1706-1538 kg/ m^3
Kinematics Viscosity	6.502×10^{-6} m^2/s
Specific Heat (solid-liquid)	2060-2230 J/kg K
Thermal Conductivity(solid-liquid)	1.09-0.54 W/m K
Latent Heat of fusion	170 kj/kg

3.2 Computational Model

The domain of the considered problem is presented in Fig. 8. A spherical glass enclosure under the gravitational field with a wall thickness of 2 mm partially filled with solid $CaCl_2 \cdot 6H_2O$ and the remaining volume occupied by air. It may be noted that the fluid flow and heat transfer in the enclosure is axisymmetric around the vertical axis of the sphere. In the initial state, the solid PCM fills 85% of the enclose space. The remaining 15% domain in the enclosed space is used for PCM volume expansion during its phase transition from solid to liquid. The initial temperature of the entire system is 23 °C.

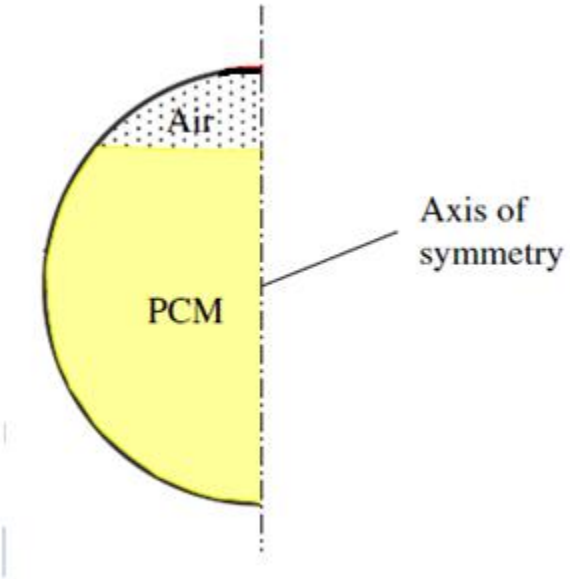

Fig. 8. Schematic of Computational Domain

The following assumptions were considered:

(1) Both air and solid/liquid PCM are homogeneous and isotropic;

(2) The liquid phase PCM is a viscous Newtonian fluid;

(3) The flow is laminar and has no viscous dissipation;

(4) The melting process is axisymmetric;

(5) The density of the PCM varies linearly in the melting temperature region from 28°C to 30°C;

A density-temperature relation is used for air:

$$\rho = 1.2 \times 10^{-5} T^2 - 0.01134T + 3.4978$$

3.3 Computational Procedure

3.31 Flow Solver

The software Ansys-Fluent was used in the simulations of this study. Fluent has two type of solver: a density-based solver and a pressure-based solver. The density solver is applicable when there is a strong coupling, or interdependence, between the density, energy, momentum, and species equations; for example, high speed compressible flow with combustion. However, the pressure based solver is applicable for a wide range of flows, especially low speed incompressible flows. Since all of the numerical simulations conducted in this study involved a phase change process, and the fluids in these simulations were assumed to be incompressible, the pressure-based solver was utilized.

These pressure-based solvers employ algorithms that belong to a general class of methods called the projection methods in which the conservation of mass within the velocity field is achieved by solving a pressure equation [19]. The pressure-based solver uses a solution algorithm

where the governing equations are solved sequentially, segregating from one another; therefore it is also called the segregated algorithm. Because the governing equations are non-linear and coupled, the solution loop must be carried out sequentially and iteratively until convergence is obtained. A flow chart of this process is presented in Fig. 9. Due to the way the governing equations are discretized for a pressure-based solver, the pressure and velocity field become coupled [19].

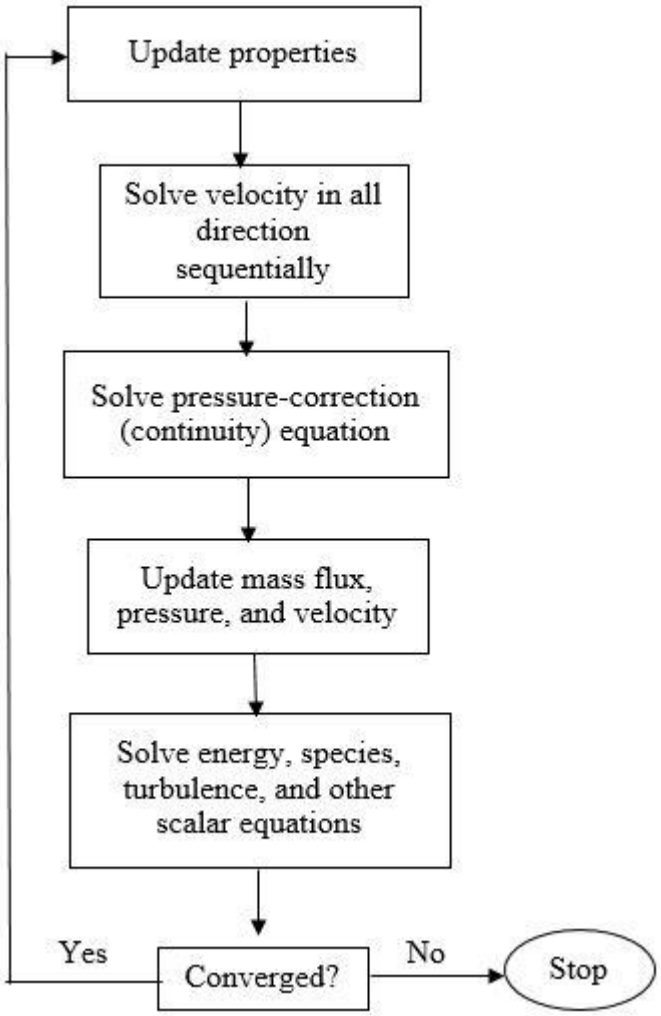

Fig. 9. Flow Chart of Pressure Based Segregated Algorithm

3.32 Enthalpy Porosity Method

In order to describe the PCM system with a moving internal interface, there are two methods to track it numerically: explicitly and implicitly. The most common method is the so-called "Enthalpy Porosity Method" first developed by V.R. Voller [20-22]. This method indirectly tracks the progression of the solid-liquid interface by using a parameter named liquid fraction, γ. In this method, the porosity in each cell is set equal to the liquid fraction in that cell. Accordingly, the porosity is zero inside the fully solid region, while porosity equals to one inside the fully liquid region. The liquid fraction is defined as:

$$\gamma = \begin{cases} 0 & T < T_s \\ \frac{T-T_s}{T_l-T_s} & T_s < T < T_l \\ 1 & T > T_l \end{cases} \quad (1)$$

Where T is the local temperature, and T_s and T_l means solid state and liquid state temperature of the phase change material, respectively. A value of $\gamma = 0$ corresponds to a solid region while a value of $\gamma = 1$ defines a liquid region, and a value of $0 < \gamma < 1$ represents the mushy zone (partially solidified region). Considering the liquid fraction γ, then the governing equations can be expressed as:

$$\frac{\partial \rho}{\partial t} + \frac{\partial}{\partial x_i}(\rho u_i) = 0 \quad (2)$$

$$\frac{\partial}{\partial t}(\rho u_i) + \frac{\partial}{\partial x_j}\left(\rho u_j u_i\right) = \mu \frac{\partial^2 u_i}{\partial x_j \partial x_j} - \frac{\partial p}{\partial x_i} + \rho g_i + S_i \quad (3)$$

$$H = h_{ref} + \int_{T_{ref}}^{T} C_p \, dT + \gamma L \quad (4)$$

$$\frac{\partial}{\partial t}(\rho H) + \frac{\partial}{\partial x_i}(\rho u_i H) = \frac{\partial}{\partial x_i}(k \frac{\partial T}{\partial x_i}) \quad (5)$$

In these equations, ρ is density, k is thermal conductivity, S_i is a momentum source term, u_i is the velocity component, μ is viscosity, H is total enthalpy, h_{ref} is the reference enthalpy, C_p is specific heat, γ is liquid fraction, and L is latent heat.

The "Enthalpy Porosity Method" makes it possible to calculate the process that occurs inside the solid PCM (conduction), liquid PCM (convection), and air (convection) simultaneously, as well as it considers the moving boundary due to PCM's continuous transformation from solid phase to liquid phase, as well as the solid sinking process in the melt.

3.33 Volume of Fluid Method

In order to study the compression of an internal void space resulting from the volumetric expansion of the PCM upon melting, the above set of governing equations for the solid-liquid phase change must be extended to multiple phases. The Ansys-Fluent offers three different multiphase models. However, in order to describe the PCM-air system with a moving internal interface, only the "Volume of Fluid" (VOF) model could be used due to its unique ability of tracking the moving interface between PCM and air. In this study, based on Equation (1), if the n^{th} fluid's volume fraction is denoted as α_n, then one could conclude the following three conditions can be established by the ideal of "Enthalpy Porosity Method":

(i) If $\alpha_n = 0$, the cell of the n^{th} fluid is empty;

(ii) If $0 < \alpha_n < 1$, the cell contains the interface between the n^{th} fluid and one or more other fluids;

(iii) If $\alpha_n = 1$, the cell of the n^{th} fluid is full

Thus, the properties of any given cell are either purely representative of one of the media, or representative of a mixture of the media, depending on the value of the volume fraction, α_n. As a result, the continuity equation, Eq. (2) could be rewritten as:

$$\frac{\partial \alpha_n}{\partial t} + \frac{\partial}{\partial x_i}(\alpha_n u_i) = 0 \quad (6)$$

Where α_n is volume fraction, t is time, x_i is direction in Cartesian coordinate, and u_i is velocity component.

3.34 Mushy Zone Constant

The Mushy Zone Constant is a parameter found in the Carman-Koseny equation which is used in the enthalpy-porosity formulation for modeling phase change. The enthalpy-porosity method treats the mushy region (partially solidified region) as a porous medium. The porosity in each cell is set equal to the liquid fraction in that cell. In fully solidified regions, the porosity is equal to zero, which eliminates the velocities in these regions. The Mushy Zone Constant measures the amplitude of the velocity damping: the higher this value, the steeper the transition of the velocity of the material to zero, as it solidifies. Very large values of the Mushy Zone Constant may cause the simulation diverge, while very small values will result in an unrealistic melting development. Therefore, the Mushy Zone Constant is an important parameter for accurately modelling phase change heat transfer. In the momentum equation, Eq. (3), the momentum source term, S_i ,resulting from the porosity change in the mushy zone can be expressed as:

$$S_i = -A(\gamma)u_i \quad (7)$$

$$A(\gamma) = \frac{C(1-\gamma)^2}{\gamma^3+\varepsilon} \quad (8)$$

Where $A(\gamma)$ is the "porosity function," first introduced by Brent et.al. [21]. $\varepsilon = 0.001$ is a small computational constant being introduced to avoid division by zero, and constant C refects the morphology of the melting point, this constant is usually defined as $10^4 - 10^7$. Reference 23 and 24 showed that C is an important parameter for accurately modelling phase change heat transfer; in particular, high mushy zone constant values corresponds to slower melting. Additionally, it was concluded that C and the temperature difference, ΔT, are not independent of one another in their roles of accurately modeling the melting rate. Different values of ΔT would require different values of mushy zone constant to achieve the same melt front development. In this study, a value of 100,000 was used.

3.4 Literature Results Validation

In order to validate the computational procedure and settings used in FLUENT, it is necessary to reproduce what other researchers have done and make a comparison.

In Reference 17, A. Darzi presented a study concerned with the numerical study of unconstrained solidification and melting of phase change material inside a two dimensional open rectangular cavity which was filled with Rt-27 as phase change material, and air. The schematics model of Reference 17 were described earlier in Chapter 2 and Fig. 3. Results of Reference 17 indicate that conduction heat transfer was dominant at the initial time of the melting process, due to the close contact of solid PCM and the inner surface of the container. Over time, solid PCM began to melt and the effect of heat convection became significant. During the melting process, solid PCM sank to the bottom of the cavity due to its higher density with respect to the liquid PCM. Fig. 10 shows a comparison between the present work and the results of Reference 17, based on the plot of melt fraction versus time. In Fig. 11, detailed melt fraction contours are also provided

for a better comparison. It could be observed that the results of present study are in agreement with those of Darzi et al. [17].

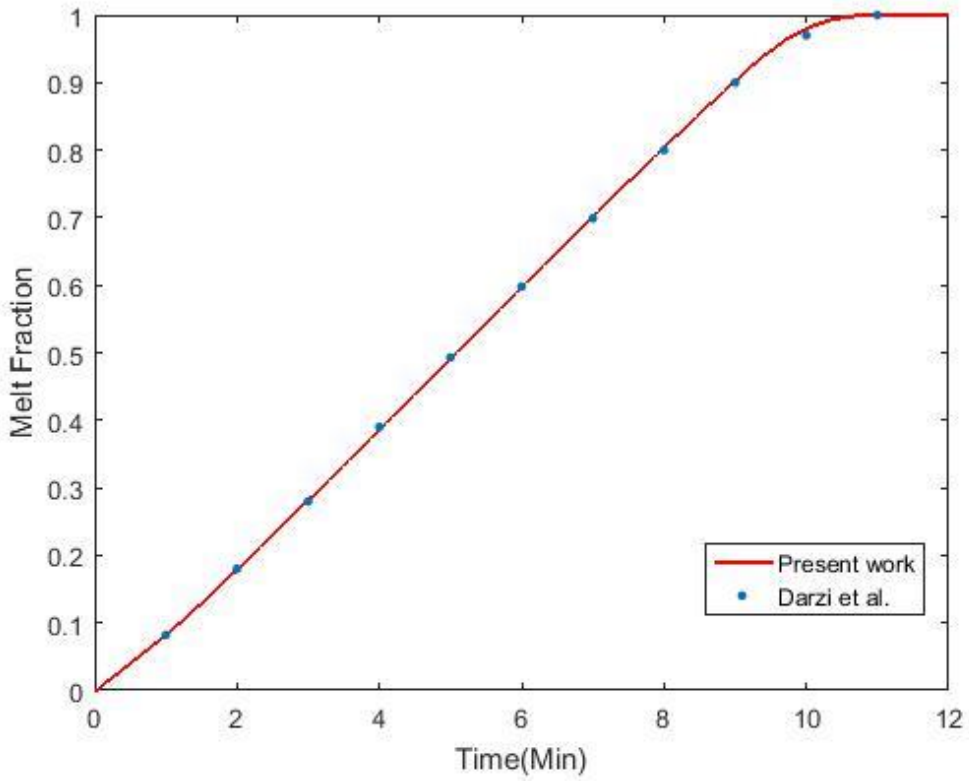

Fig. 10. Comparison of Melt Fraction Inside a 2-D Rectangle Cavity between the Present Work and Results of Darzi et al.

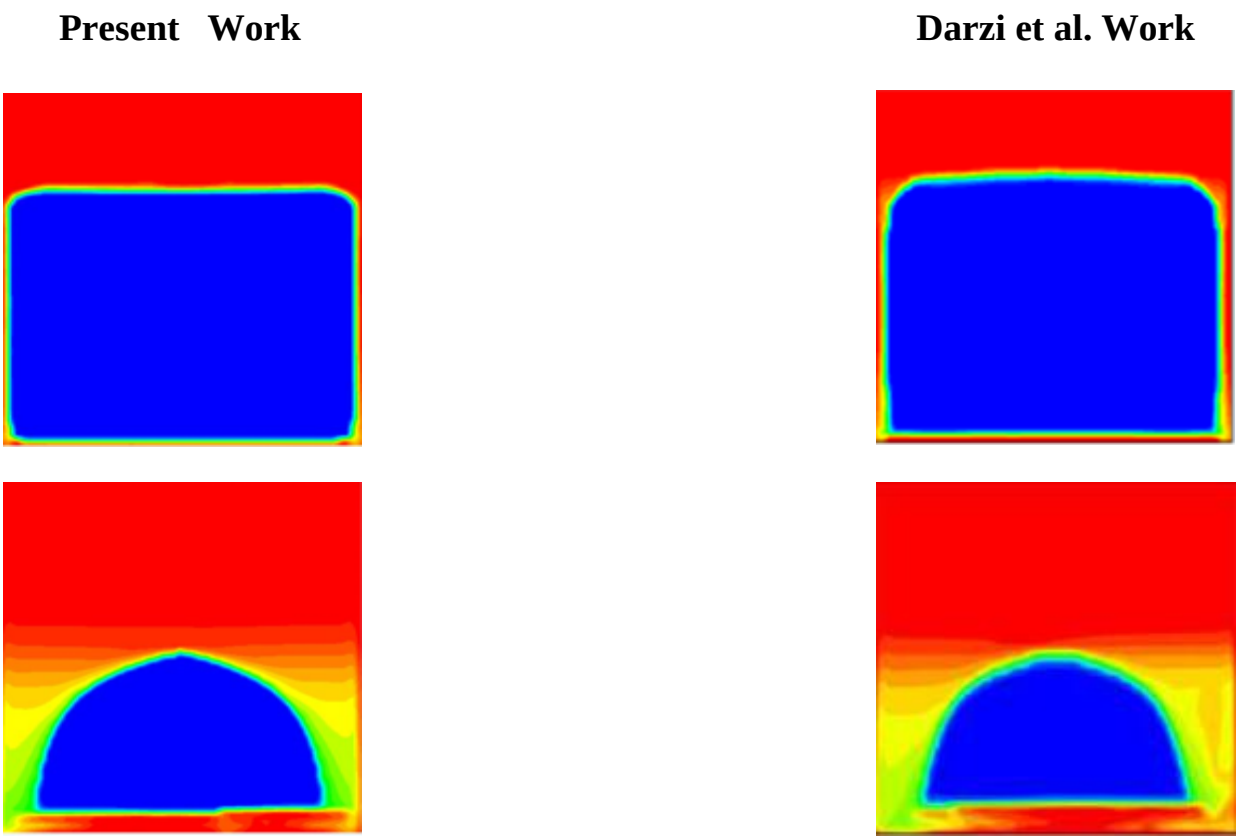

Fig. 11. Comparison of Melt Fraction between the Present Work and Darzi et al.'s Work at Times of 1 min and 6 min

Additionally, another literature validation was performed for a different geometry enclosure. In Reference 18, A. Archibold analyzed a two dimensional axisymmetric model of heat transfer and fluid flow during the melting process inside a spherical latent heat thermal storage enclosure. A void space was provided within the enclosure to take into account the volumetric expansion of the PCM. This physical model was displayed in Chapter 2 and Fig. 4. The mathematic model was solved using the "Finite-Volume Method," and the "Enthalpy-Porosity Formulation" was employed to solve the energy equation for both solid and liquid regions of PCM. In Fig. 12, the numerical results of this study are compared with the results reported by Archibold et al. [18].

Reasonably good agreement was found between the melt fraction rate by Fluent and the numerically predicted melt fraction rate from Reference 18.

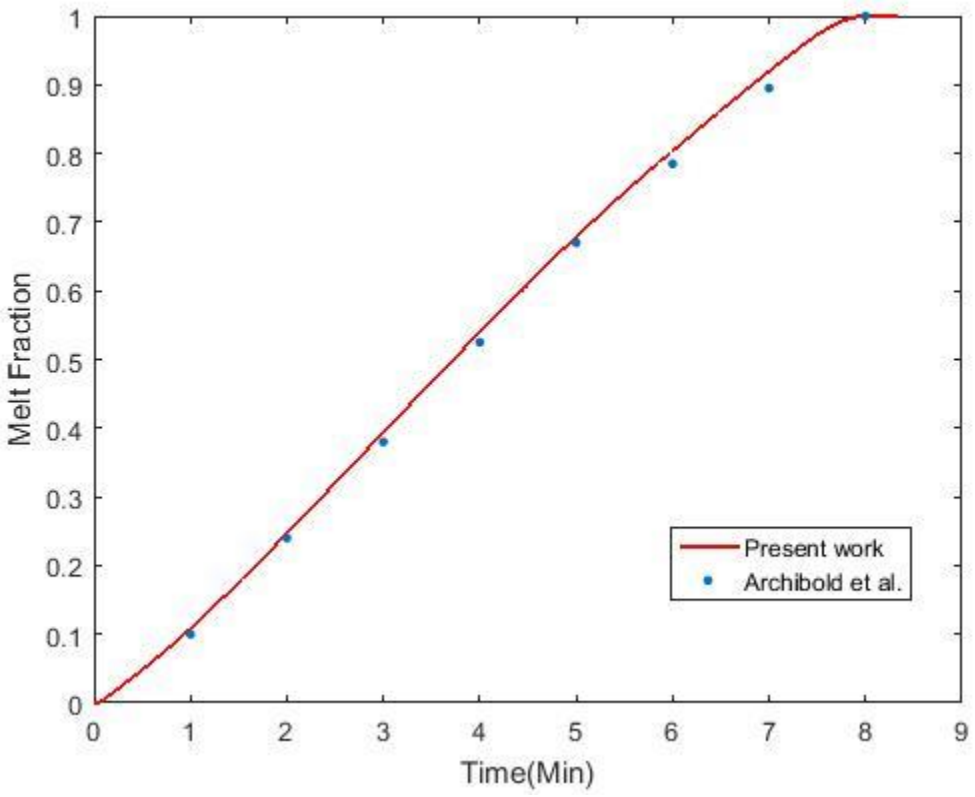

Fig. 12. Comparison of Melt Fraction Inside a Spherical Enclosure between the Present Work and Archibold et al.'s Work

CHAPTER 4: EXPERIMENTAL SET-UP AND PROCEDURE

In this study, experiments were designed specifically to validate the results achieved in the numerical investigation. A flask used in the experiment for PCM enclosure is shown in Fig. 13. The experimental set up consisted of a spherical shell with an inner diameter of 40 mm. The amount of PCM used in the experiments matches the PCM mass used in the FLUENT simulations. The PCM solid phase initially occupied 85% of the volume. In order to achieve a desired shape, the container was firstly gradually filled with liquid state PCM, then put it into an icebox, allowing the liquid PCM to solidify gradually. The material used in the experimental study, as in the numerical simulations, was calcium chloride hexahydrates. The spherical container has a "neck" that lets the air out when the PCM expands during melting.

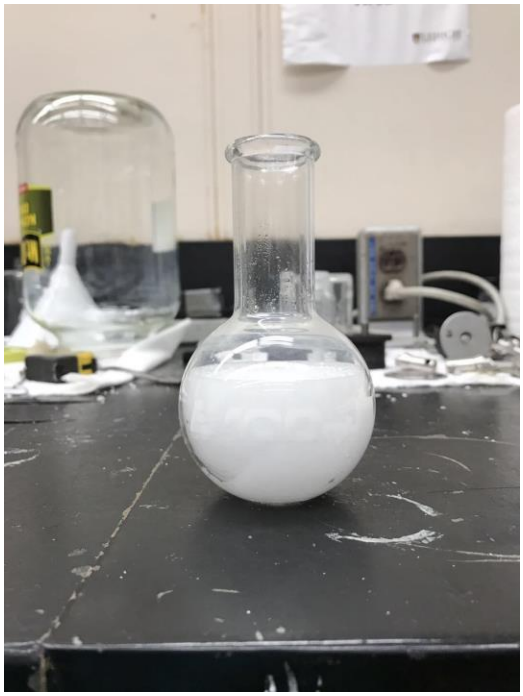

Fig. 13. Experimental Flask with PCM

The experimental set-up is shown schematically in Fig. 14 [25-26]. Experiments were performed using an experimental tank, filled with water. An electric heater was used to keep the water temperature at a set level, and its power was adjusted using a variable voltage controller. An electric stirrer was used to ensure uniform temperature of the water inside the tank. A thermocouple was used to monitor the temperature of the water at the location near the PCM container. This thermocouple was connected to a PC through a data acquisition unit. A photo of the water tank machine is shown in Fig. 15. The voltage controller, the electric motor, the electric heater, and the stirrer were all contained in the water tank system. A waterproof camera was positioned near the spherical shell to record the entire phase change process.

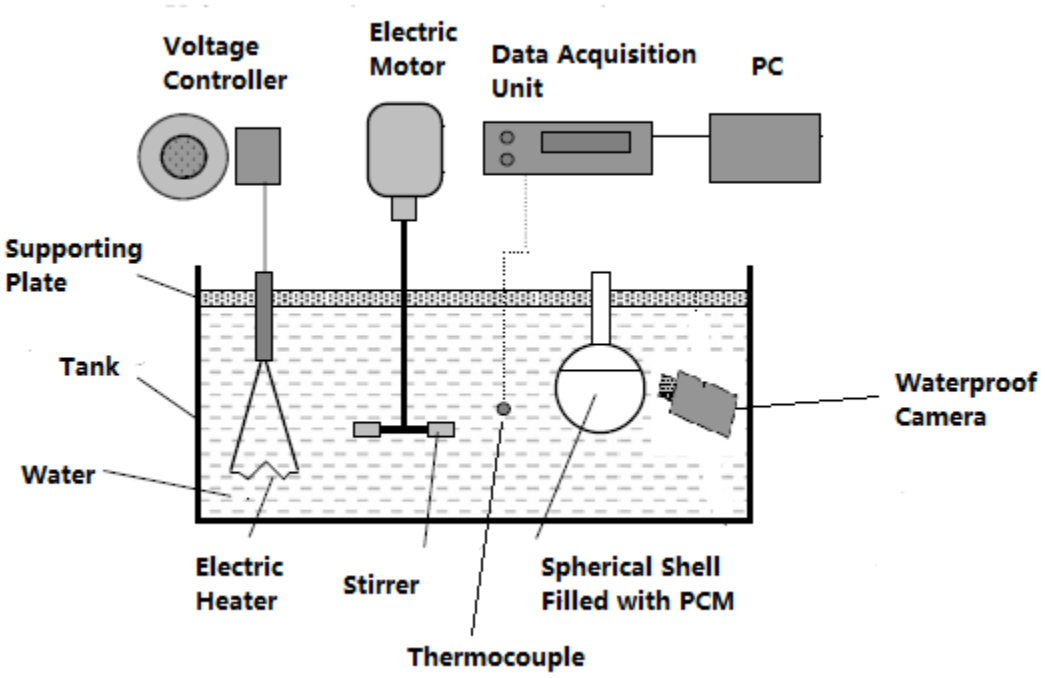

Fig. 14. Experimental Set-Up Used in the Experiment

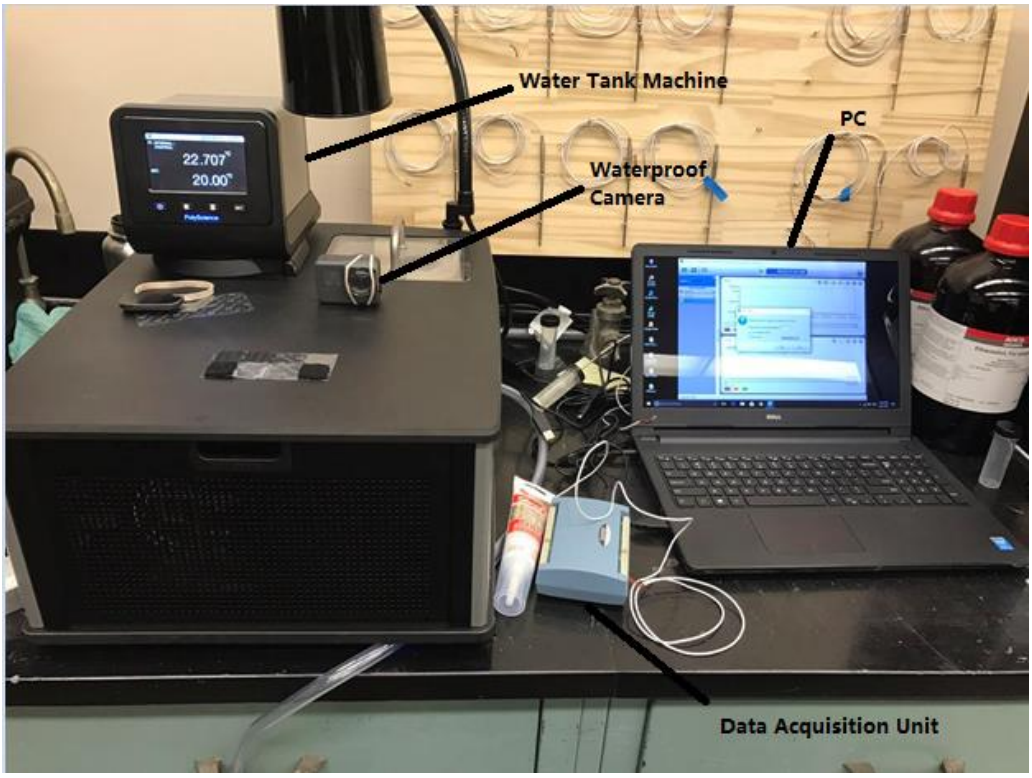

Fig. 15. Photo of Water Tank System

In a typically experiment, when the temperature of the water reached 39 °C, the spherical shell filled with the solid PCM was submerged into the water. Then, the PCM enclosure warmed up and the meting process began. Melting fraction images were recorded by the waterproof digital camera at various stages of the process. These images were analyzed and the experimental values of the melt fraction was calculated by measuring the height of solid PCM at various time instants. These results were used for validation of the numerical calculations, as reported in the next Chapter.

CHAPTER 5: RESULTS AND DISCUSSION

This chapter presents a comparison of the experimental and simulation results. A detailed sensitivity analysis of the PCM melting process is also described and discussed in this chapter, including a generalization of the melting process parameters.

5.1 Validation of the Numerical Model

5.11 Impact of Time Step and Meshing Grid Size

Numerical solutions were obtained using the software Ansys-Fluent 17.1. Definition of time step is critical for unsteady flow where the properties of the flow vary with time. Time step size is a specific time value between each iteration when solving the governing equations of unsteady flow. For example, when a 5 seconds fluid flow process is simulated with a time step size of 0.01 sec, there will be 500 iterations. In general, the more the iterations, the more accurate simulations would be achieved, because the flow properties change at every moment. Therefore, in order to capture all of the flow parametric fluctuations during simulations, it is advised to select small time step sizes. Additionally, meshing grid size also has a significant impact on simulation accuracy. After configuring a model in Ansys-Fluent, it is necessary to designate elements on this model. Meshing grid size equals to the number of elements. Because different parts on a model have different flow properties, more elements could contribute to a more accurate simulation result. In this study, the effects of time step and meshing grid size on the solutions were carefully examined in preliminary calculations, as presented in Figs. 16 and 17, respectively. The simulation model was the same as the experiment model which was described in Chapter 4.

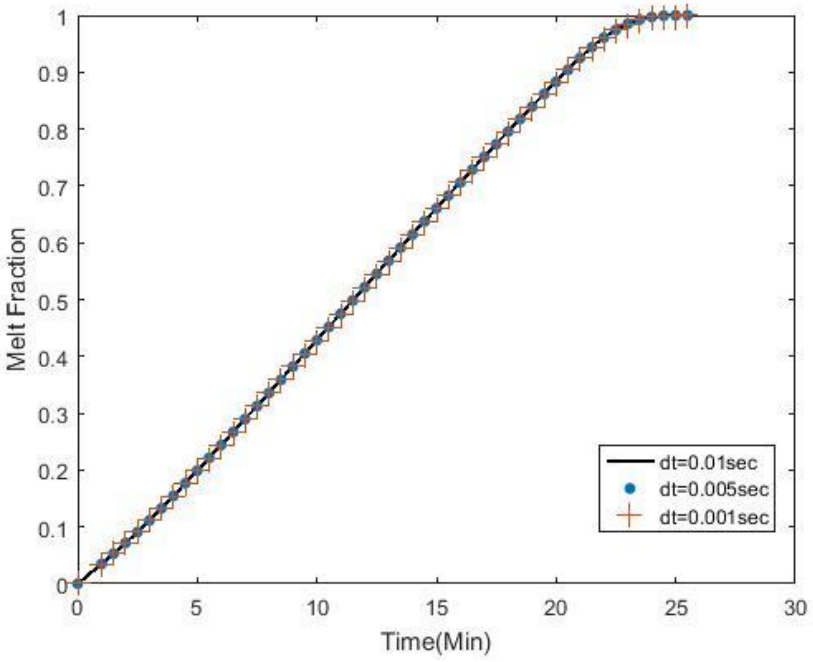

Fig. 16. Time-Step Dependence of Numerical Solutions

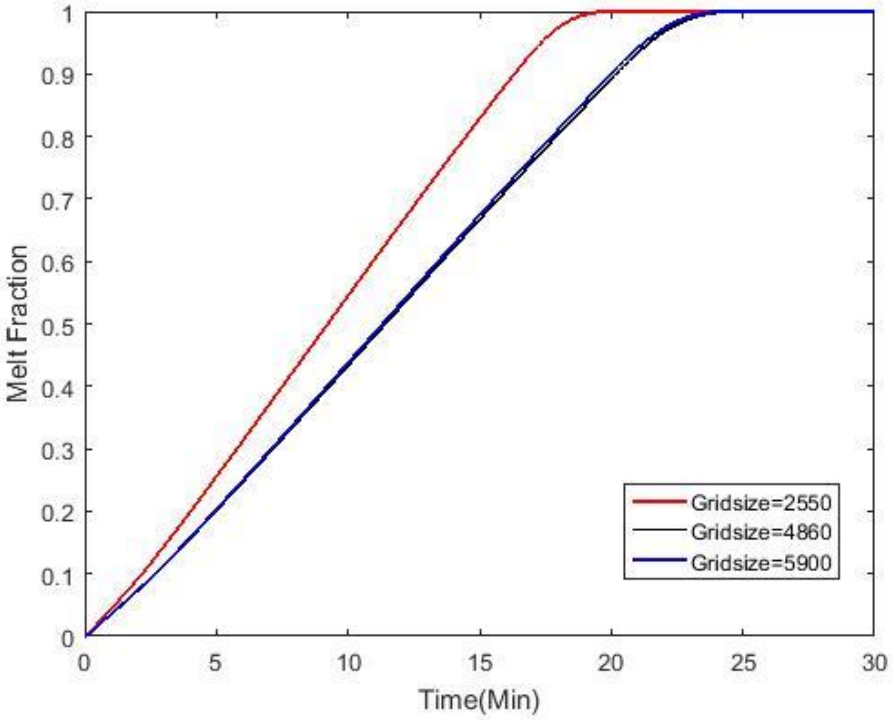

Fig. 17. Meshing Grid Size Dependence of Numerical Solutions

From Fig. 16, it can be seen that the time step size was set to as small as 0.01, 0.005, and 0.001 sec. The results obtained for the melt fraction are practically independent of the chosen time steps through the entire melting process. The meshing grid size was set to 4,860 cells for all these three time step size simulations.

The mesh grid was built in the Fluent software, with special attention paid to the PCM-air interface. The meshing grid size was chosen after careful examination of the refinement process (a method of adapting the accuracy of a solution within certain sensitive regions of simulation). Fig. 17 shows results for three different grid size, 2,550, 4,860, and 5,900 cells, respectively. It could be observed that the difference between 4,860 and 5,900 are rather small. Therefore, the time step of 0.01 sec and grid size of 4860 cells were selected for further simulations, in order to shorten the simulation time. Decreasing the time step size or increasing the meshing grid size could both contribute to longer simulation times, which was the reason why the time step size of 0.001 sec and the meshing grid size of 5,900 were not selected.

Convergence of the solution was checked at each time step during simulations. Scaled absolute residuals of 10^{-4}, 10^{-6} and 10^{-8} were used for the continuity, velocity components and energy equation, respectively. An OPTIPLEX 7010 computer was used for these simulation. This computer features eight core 3.40 GHz Inter Core i7-3770 processors and of 8 Gb installed memory. The calculation time was rather considerable, a typical case would take more than 2 days to run.

5.12 Validation with the Experimental Results

For the computer case, the enclosure was simulated to be filled with solid PCM, occupying 85% of the volume of the enclosure.

The boundary conditions for the simulation case were set at:

(i) The outer surface temperature of the enclosure was set to a constant whose value was 10°C higher than the mean melting temperature of the PCM;

(ii) The top surface pressure of the enclosure was maintained at atmosphere pressure during the entire simulation process;

The initial temperature condition for the simulations was set at 23°C.

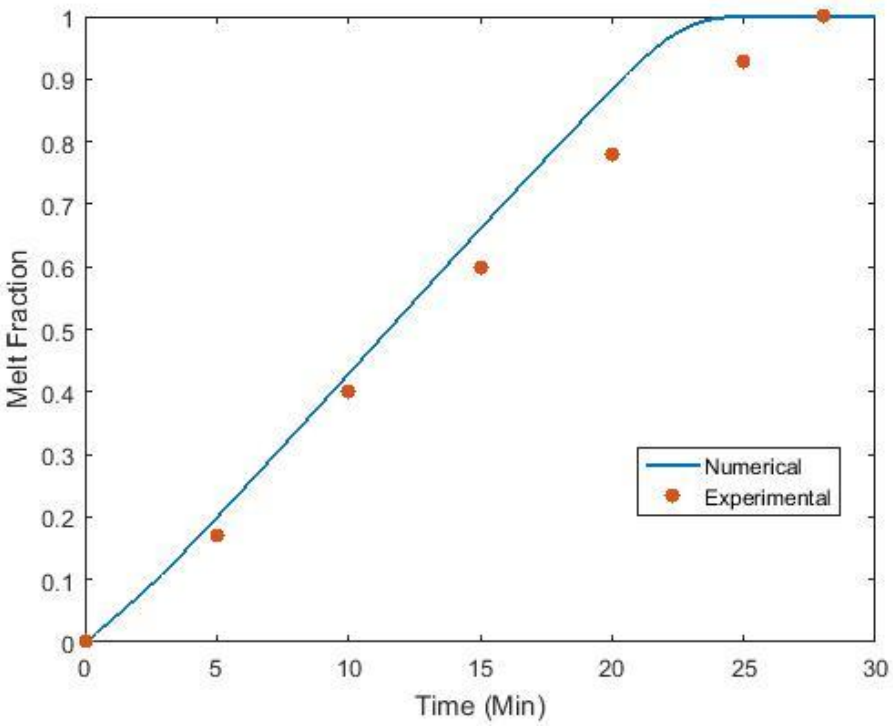

Fig. 18. Comparison of Experimental and Numerical Melt Fraction

A measured and simulated melt fractions vs. time plot is shown in Fig. 18. In Fig. 18, it can be observed that the melting time predicted by the simulation is shorter than the corresponding time measured in the experiment. This may be due to the temperature of the water bath kept constant during the experiment, taking some time for the outer surface of the container to warm up from room temperature to the temperature set point. This compares to the simulation where a

high value temperature was directly set to the outer surface of the shell. Thus, an additional thermal resistance existed in the experiments that did not exist in the simulations. Additionally, the value of the glass thermal conductivity was taken from the literature, but it could be higher than the reported value. The agreement between measured and estimated melt fraction of Fig 18 is reflectively good in terms of the trend and total melting time (25 min melt time for the simulation vs. 28 min melt time for the experiment). Additionally, Fig. 19 shows results from the visualization of calcium chloride melting, as obtained during the experiment, at 2, 5, 10, 15, 20, and 23 min since the start of the process. Fig. 20 shows corresponding results of the simulated phase distribution for the same times as in Fig. 19. It could be seen from both Fig. 19 and 20 that the solid phase indeed descends to the bottom of the shell during the melting process. At the beginning of the melting process, heat is transferred by conduction through the enclosure wall due to the temperature difference between the wall and the initial temperature of the system. Then, solid PCM near the wall absorbs heat and its temperature increase up to the melting point. At this stage, heat conduction was the dominant mechanism. The absorbed heat is then used for phase change from solid state to liquid state. Over time, the thickness of the liquid PCM became larger, with gravity and the difference between solid and liquid density of the PCM forcing the solid phase to sink towards the bottom of the enclosure and push up hot liquid PCM, which enhances the convection and accelerates the melting rate.

Comparing simulation results with experiment results, one could see quantitatively good agreements on the aspect of total melting time and detail melting fractions. It could be concluded that the numerical approach yields valid results for the description of PCM phase change.

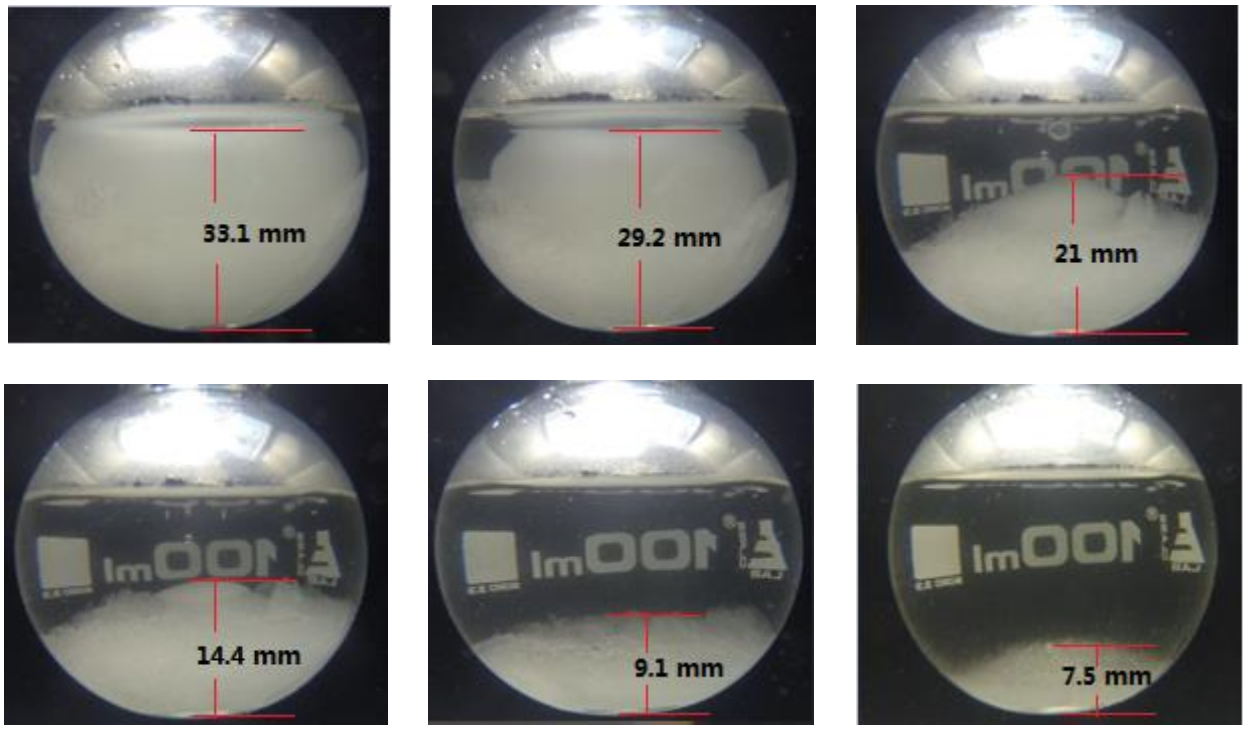

Fig. 19. Experimental Melting Fractions

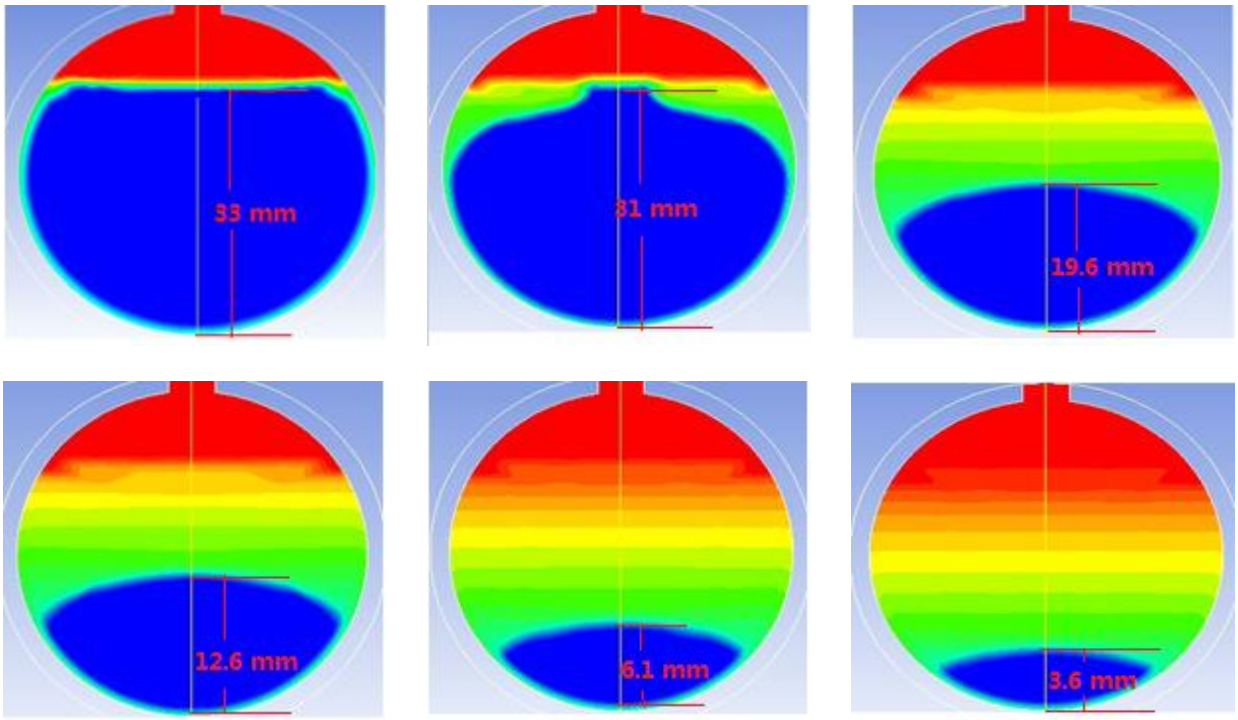

Fig. 20. Numerical Melting Fractions

5.2 Sensitivity Analysis

After validating the numerical approach and simulation settings in Fluent, a sensitivity analysis was performed in order to get a generalized solution of PCM melting process. Six different cases were run as summarized in Table 6. The effect of the Grashof Number on the melting and heat transfer for a constant Stefan number was evaluated by comparing the first three case, where the shell diameter was varied from 40 to 80 mm. Cases 1, 4, and 5 were considered in order to assess the role of the outer surface temperature of the PCM enclosures on the melting process.

Table 6. Analyzed Cases

Case number	R (mm)	ΔT (K)	Gr_R	Ste	Pr
1	20	10	8×10^6	0.132	1.4
2	30	10	2.7×10^7	0.132	1.4
3	40	10	6.4×10^7	0.132	1.4
4	20	5	4×10^6	0.066	1.4
5	20	15	1.2×10^7	0.198	1.4

The non-dimensional numbers were defined as:

$$Gr_R = \frac{g\rho^2\beta\Delta T R^3}{\mu^2} \quad (9)$$

$$\text{Ste} = \frac{C_p\Delta T}{L} \quad (10)$$

$$\text{Pr} = \frac{C_p\mu}{k} \quad (11)$$

Where g is gravity; ρ, μ, C_p, and k are density, dynamic viscosity, specific heat, and thermal conductivity of liquid PCM, respectively; ΔT is the difference between the outer surface temperature and the PCM mean melting temperature, R is the radius of PCM enclosure, L is the latent heat of the PCM, and β is the volumetric expansion coefficient.

Numerically predicted liquid mass fractions as a function of time for cases 1-3 are presented in Fig. 21. A faster melting process takes place in the smaller size capsules. The total melting time were 25, 38, 54 min for Cases 1, 2, and 3, respectively. In order to isolate the effect of container size and investigate the role that natural convection heat transfer (Grashof Number) plays in the melting process of calcium chloride hexahydrate under constant Stefan Number, the liquid mass fractions for Cases 1-3 are presented in Fig. 22, as a function of a dimensionless time (defined as the product of the Stefan and Fourier Numbers).

The expression for Fourier Number is noted:

$$\mathrm{Fo} = \frac{kt}{\rho C_p R^2} \tag{12}$$

Where ρ, C_p, and k are density, specific heat, and thermal conductivity of liquid PCM, respectively, R is the radius of the enclosure, and t is time.

In Fig. 22, it can be observed that a faster melting process occurs with an increase in the Grashof Number from 8×10^6 to 6.4×10^7 for a constant Stefan number of 0.132. It is important to mention that the Fourier number varies inversely as the square of the diameter of the shell. Therefore, the Fourier number of a smaller diameter case is higher than the value obtained for a larger diameter case. This can be seen in the reverse trend as seen in Fig. 22 when compared to Fig. 21.

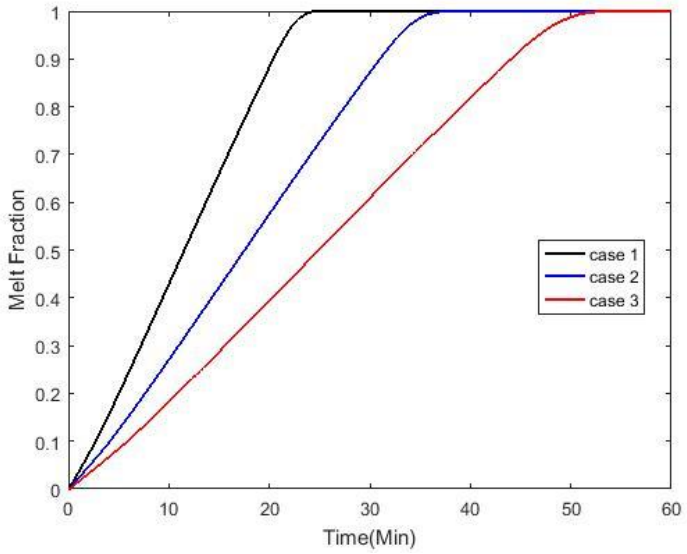

Fig. 21. Melt Fraction for Cases 1-3

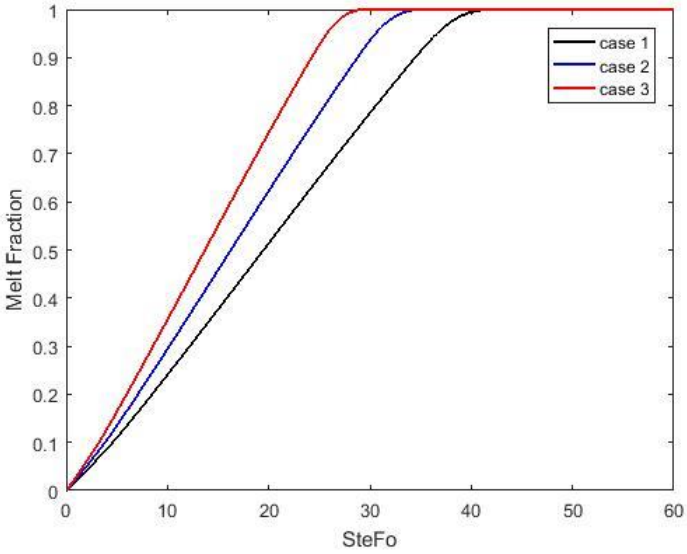

Fig. 22. Grashof Number Effect on Melt Fraction for Cases 1-3

Simulated heat transfer rates at the outer surface of the enclosure for Cases 1-3 are presented in Fig. 23. Results in Fig. 23 indicate that higher values of heat transfer rate are obtained in the first several seconds for all three cases because of the high temperature difference between the outer surface of the shell and the solid PCM which is in direct contact with the inner shell wall. As

the temperature of solid state PCM increases up to the melting point, it begins to melt and changes to liquid state. When the first layer of liquid PCM is created, the heat transfer rate of all these three cases decreases drastically due to the low thermal conductivity of the liquid layer. As the liquid PCM layer gets thicker and the contribution of heat convection becomes significant, the decrease rate turns to be mild. Because the temperature difference between the outer surface and the system continually becomes smaller during the melting process, a progressively reducing trend is observed in all the curves from the beginning towards an thermal equilibrium state where heat transfer rate equals to zero. In the analysis of Cases 1-3, the instantaneous heat transfer rate was found to be enhance with an increase in the Grashof Number (from 8×10^6 to 6.4×10^7) of the system.

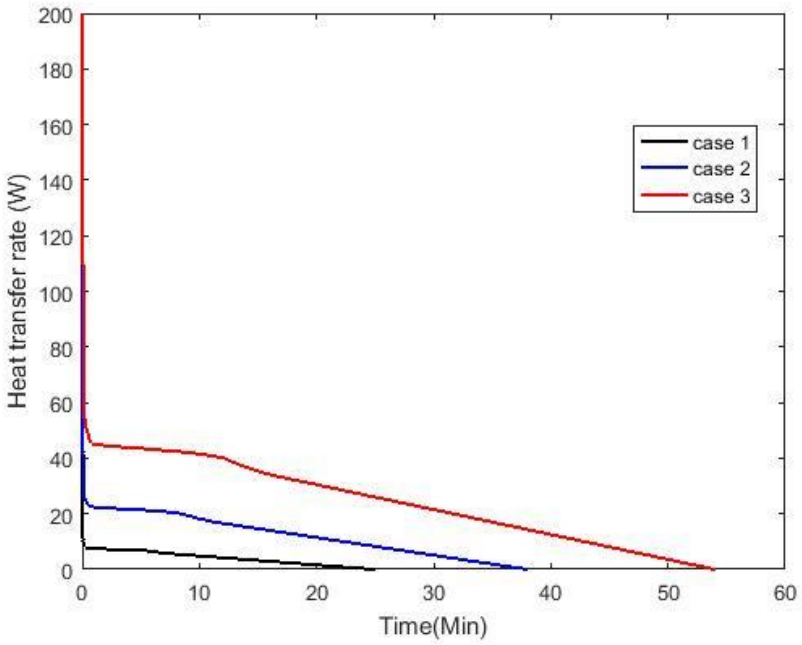

Fig. 23. Heat Transfer Rate for Cases 1-3

The effect of the outer surface temperature of the enclosure on PCM thermal performance is presented in Figs. 24 and 25. The predicted melt fractions of the Cases 1, 4, and 5 with equal geometry but different surface boundary temperature, are shown in Fig. 24. It could be observed that faster melting is achieved when the outer surface temperature increases. The total melting time

for Cases 1, 4, and 5 are 23.7 mins, 50 mins, and 13.5 mins, respectively. The percentage decrease in t total melting time is 52.6% for Case 1, and 72.3% for Case 5 when compared to the corresponding value for Case 4. Fig. 25 illustrates the heat transfer rate at the outer surface of the enclosure for Cases 1, 4, and 5. It was found that an increase in the Grashof and Stefan Number could enhance the heat transfer rate in the first several seconds. After this period, an opposite trend is observed in the curves and is related to the fact that faster thermal equilibrium is reached by the enclosure with the higher outer surface temperature. It should be noted that with the increase in the outer surface temperature both the Grashof and Stefan Number increase. Thus, the changes in Grashof and Stefan Number correlate with the aforementioned behavior.

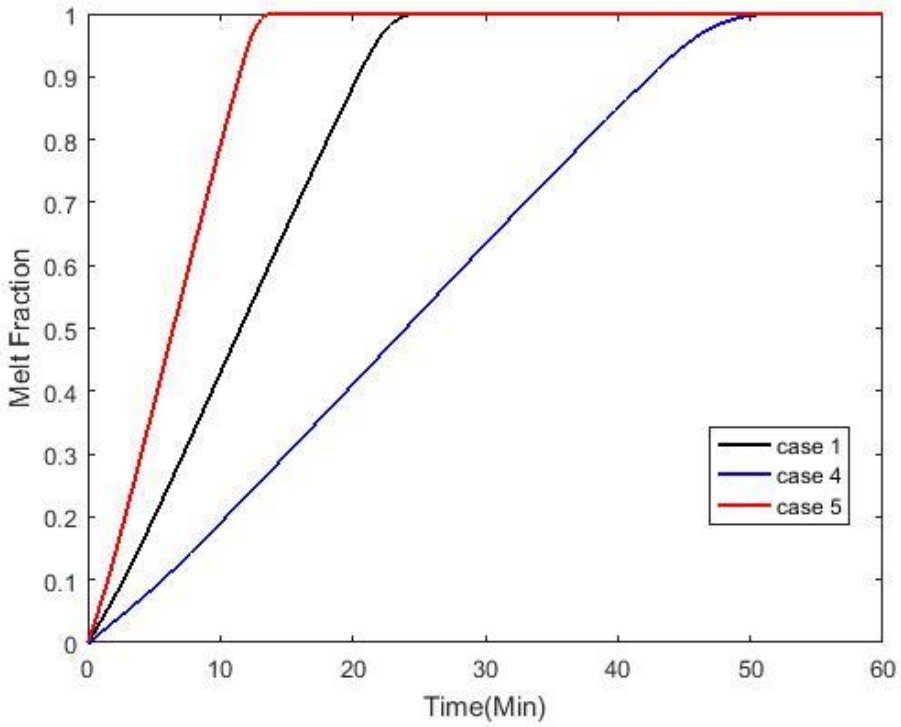

Fig. 24. Melt Fraction for Cases 1, 4, and 5

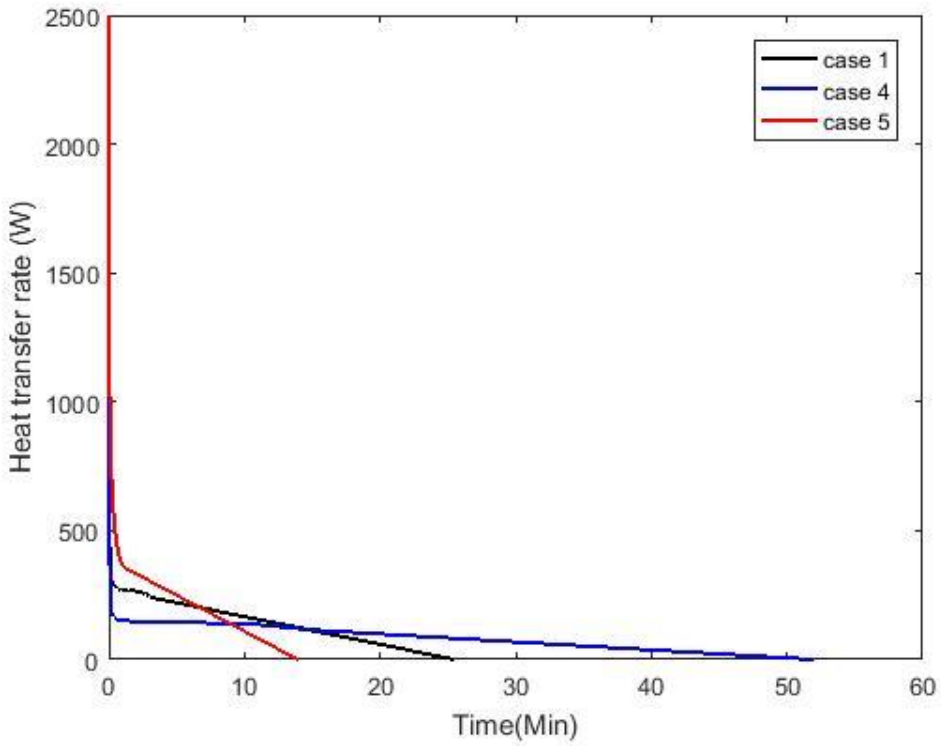

Fig. 25. Heat Transfer Rate for Cases 1, 4, and 5

5.3 Generalization

The results presented in Figs. 21-25 and previously discussed show the similarity in melting behavior under different geometrical and thermal parameters of the system. It is thus worth attempting to perform a dimensional analysis in order to obtain generalized results for the melting process.

There are two dependent dimensionless parameters that can be used: the melt fraction of the PCM, defined as the current melted mass divided by the total mass of the PCM, and the Nusselt Number, which is defined as:

$$\mathrm{Nu} = \frac{q}{\Delta T} \cdot \frac{R}{k} \tag{13}$$

Equation (13) is based on heat flux, q, the temperature difference between the wall and the PCM mean melting temperature, ΔT, the shell radius R, and the thermal conductivity of the PCM, k. It should be noted that melt fraction rather reflects the amount of heat stored in the system at every moment of the melting process, while the Nusselt Number shows an instantaneous snapshot of the process at the same moment. Therefore, these two parameters supplement each other.

In Fig. 22, three curves were plotted merge together during the very initial period when heat conduction is the dominate mechanism. This may infer that a combination of the Fourier and Stefan Numbers would have been sufficient to describe melting promoted by heat conduction. It can also be seen from Fig. 22 that when the melt fraction is plotted vs. the product, SteFo , of the Fourier Number and Stefan Number, no generalization is achieved, although the different curves come closer together when compared to the curves in Fig. 21. In order to appropriately correlate the Cases results and develop an suitable expression, which characterizes the phase change of the PCM (Stefan Number), the natural convection (Grashof Number), and the dimensionless time (Fourier Number). It is proposed to arrange an expression of Fo$Ste^{a}Gr^{b}$. A careful analysis of the dimensionless group where a $= \frac{1}{3}, b = \frac{1}{4}$ led to the generalized results presented in Figs. 26, 27, and 28. Fig. 26 shows the melt fractions vs. a combination of the Fourier, Stefan, and Grashof Number, expressed as Fo$Ste^{1/3}Gr^{1/4}$, for all cases considered in this study. It could be seen that all curves practically merge into a single curve. Analysis of the results of Fig. 26 yields the following expression for the melt fraction:

$$\mathrm{MF} = 1 - \left(1 - \frac{FoSte^{\frac{1}{3}}Gr^{\frac{1}{4}}}{2.8}\right)^{2.35} \qquad (14)$$

This correlation is also shown in Fig. 26.

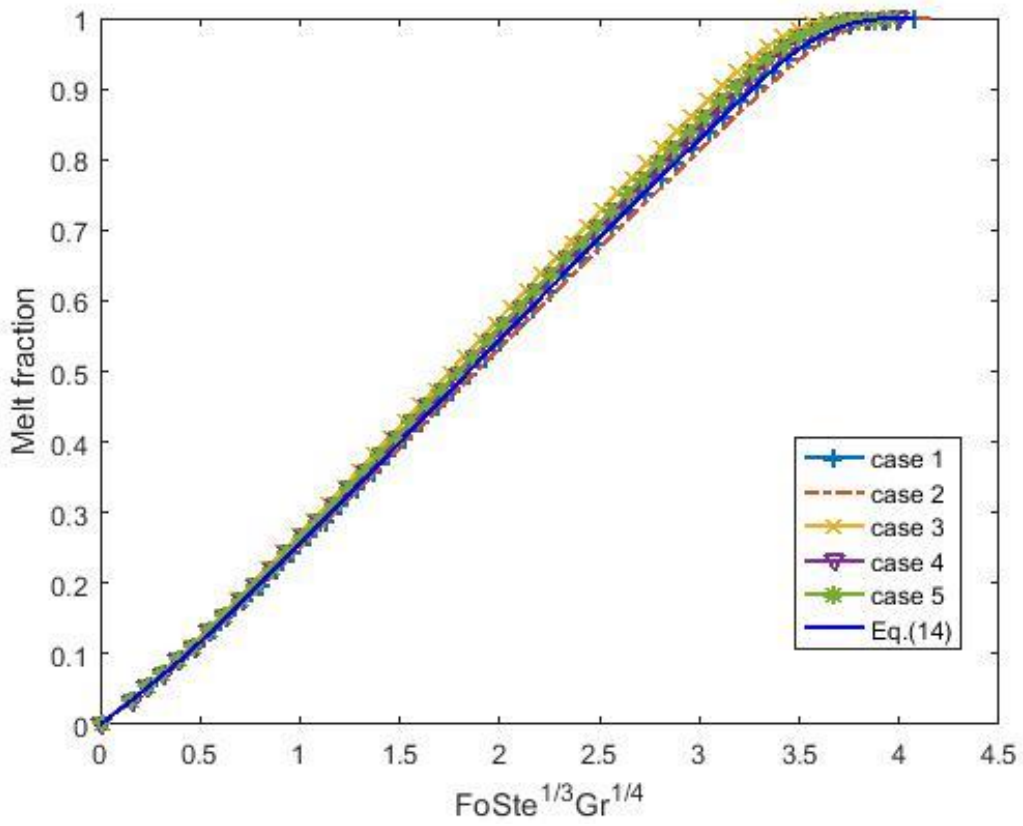

Fig. 26. Generalized Results for All Simulated Cases: Melt Fractions

Fig. 27 shows the dimensionless integral heat flux from the outer surface of the PCM enclosure vs. the same combination of the Fourier, Stefan, and Grashof Numbers, Fo$Ste^{1/3}Gr^{1/4}$. The Nusselt Number was normalized using the Grashof Number. The exponent of the Grashof Number was chosen based on laminar natural convection conditions, as indicated in Reference 18. It can be seen that distinct curves are formed corresponding to the different values of the Stefan Number in Fig. 27. Additionally, Fig. 28 shows that these curves can be further merged when the Nusselt Number is additionally normalized using the Stefan Number. The exponent of the Stefan Number was also selected based on the laminar flow conditions [18].

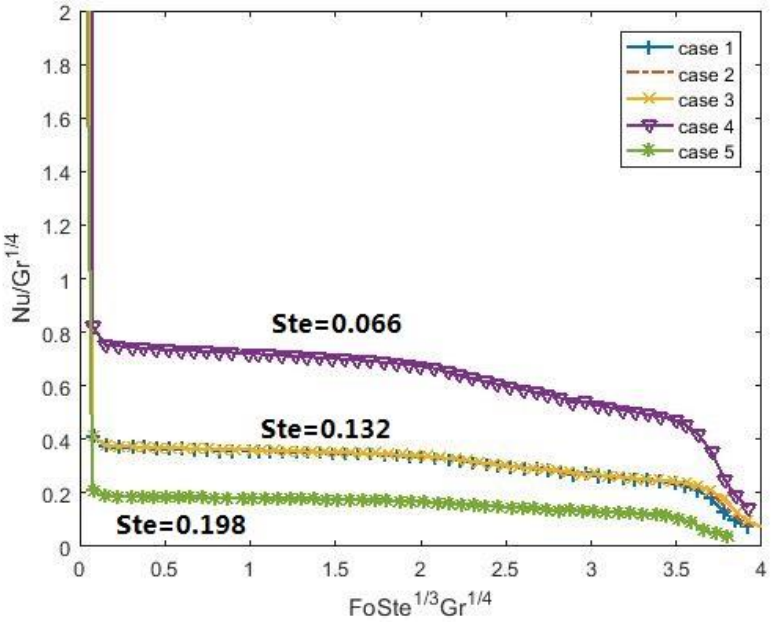

Fig. 27. Generalized Result for Simulation Cases (Stefan Number as a Parameter)

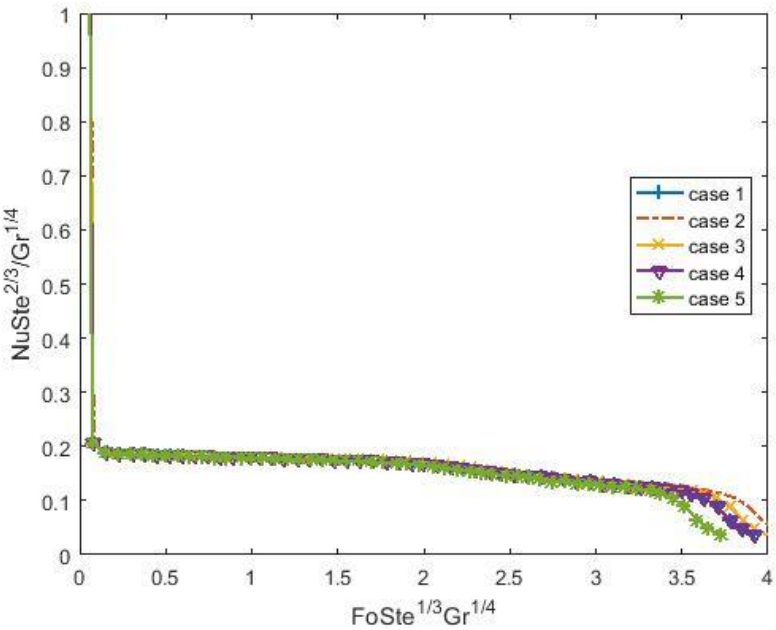

Fig. 28. Generalized Result for Simulation Cases (Nusselt Number Normalized with Stefan Number)

The last results presented in this Chapter were obtained for cases in which air was allowed to flow out of the enclosure to accommodate the PCM expansion. In industrial applications, the shell may be sealed, and the air compressed. Additionally, it was also assumed that the PCM-air interface was initially horizontal and flat. In a real situation, its shape will be determined by the solidification process. However, it is believed that the trends discovered in this thesis are quite general, and the results of the analysis performed herein might be valid also when these additional features are taken into account.

CHAPTER 6: CONCLUSIONS AND RECOMMENDATIONS

In this study, the melting process of a phase change material in spherical geometry was studied experimentally and numerically. This study took into account together the phenomena of convection in the liquid phase, volumetric expansion due to melting, motion of solid phase, and close contact melting. The phase change material used in this study is a commercially available salt hydrate with a relatively lower melting point than used in other researches related to heat storage systems. The experimental study included visualization of the melting process. The simulations provided detailed meting contours inside the system which were compared with the experimental results.

After a sensitivity analysis, a dimensional analysis of the results was performed and presented in terms of the Nusselt Numbers and PCM melt fractions vs. an appropriate combination of the Fourier, Stefan, and Grashof Numbers, to describe the heat transfer mechanism with solid sinking phenomenon. This analysis led to a generalized analytical description of process.

The following conclusions are drawn:

(1) Based on the flow pattern and melting interface evolution during the melting process of calcium chloride hexahydrate for a fixed Stefan Number (Ste=0.132), it was found that an increase in the Grashof Number from 8×10^6 to 6.4×10^7 enhances the heat transfer process, which means the melting rate increases. Additionally, the corresponding heat transfer rate was found to increase with increases in the Grashof Number.

(2) The combined effect of the Grashof and Stefan Numbers with an increase in the outer surface temperature generated a 72.3% reduction in total melting time for a case where the temperature difference between the outer surface of PCM enclosure and the initial system temperature is 15°C as compared to the corresponding total melting time of a case where

the temperature difference between the outer surface of PCM enclosure and the initial system temperature is 5°C.

(3) Appropriate dimensionless variables based on a combination of the Fourier, Grashof and Stefan numbers could lead to a generalized correlation for the liquid mass fraction as well as the heat transfer rate during the melting process of calcium chloride hexahydrate.

However, there are still some point need further investigations:

(1) It was noted that the melting process of solid phase PCM was observed to follow in general the same pattern in all simulated cases in this study. However, when the temperature difference between the initial system and outer surface of the enclosure becomes higher than 20°C, the melting pattern of the solid phase PCM becomes totally different. Holes at the surface of solid PCM were observed during the melting process, and these holes become deeper until the solid PCM break into several parts. This will require a more detailed study to investigate applications that exceed the temperature range.

(2) In this thesis, an open enclosure was used to let the air go outside of the container during the PCM's volumetric expansion. However, in industrial applications, the PCM enclosures are usually sealed, and air compressed. Modeling and experimental setup according to a more actual application would provide more realistic result for the design of practical PCM thermal energy storage system in this temperature range.

REFERENCES

[1] Gil, A., Medrano, M., Martorell, I., Lazaro, A., Dolado, P., Zalba, B., and Cabeza, L. F., 2010, "State of the art on high temperature thermal energy storage for power generation. Part 1—Concepts, materials and modellization," Renewable and Sustainable Energy Reviews, 14(1), pp. 31-55.

[2] Kuravi, S., Trahan, J., Goswami, D. Y., Rahman, M. M., and Stefanakos, E. K., 2013, "Thermal energy storage technologies and systems for concentrating solar power plants," Progress in Energy and Combustion Science, 39(4), pp. 285-319.

[3] Sharma, A., Tyagi, V. V., Chen, C. R., and Buddhi, D., 2009, "Review on thermal energy storage with phase change materials and applications," Renewable and Sustainable energy reviews, 13(2), pp. 318-345.

[4] D. Gao, T. Deng, 2013, "Energy storage: Preparations and physicochemical properties of solid liquid Phase change materials for thermal energy storage," A. Mendez-Vilas (Ed.), Mater. Process. Energy Commun .Curr. Res, Technol. Pp. 32-44.

[5] Kenisarin, M., and Mahkamov, K., 2007, "Solar energy storage using phase change materials," Renewable and Sustainable Energy Reviews, 11(9), pp. 1913-1965.

[6] Farid, M. M., Khudhair, A. M., Razack, S. A. K., and Al-Hallaj, S., 2004, "A review on phase change energy storage: materials and applications," Energy Conversion and Management, 45(9–10), pp. 1597-1615.

[7] Paksoy, H., Mehling, H., and Cabeza, L., 2007, "Phase Change Materials and Their Basic Properties," Thermal Energy Storage for Sustainable Energy Consumption, Springer Netherlands, pp. 257-277.

[8] Lane, G. A., 1983, "Solar Heat Storage: Latent Heat Material, Volume I, Background and Scientific Principles, " CRC Press, Florida.

[9] Lane, G. A., Lee, M., Collins, J. W., Aubrecht, D. M., Sperling, R. A., Solomon, L., Ha, J.-W., Yi, G.-R., Weitz, D. A., and Manoharan, V. N., 1986, "Solar Heat Storage: Latent Heat Material, Volume II, Technology Synchronized reinjection and coalescence of droplets in microfluidics," Lab on a Chip, 14(3), pp. 509-513.

[10] K.T. Adref, I.W. Eames, 2002, "Experiments on charging and discharging of spherical thermal (ice) storage elements," Int. J. Energ, pp. 949-964.

[11] Wenzhen, C. Shangmo, C. Zhen, L. Wangmin, G., 1993, "Study of Contact Melting Inside Isothermally Heated Vertical Cylindrical Capsules," Int. J. Thermal Science.

[12] M. Bareiss, H. Beer, 1984, "An analytical solution of the heat transfer process during melting of an unfixed solid phase change material inside a horizontal tube," Int. J. Heat Mass Transfer, pp. 739-746.

[13] T. Saitoh, K. Katoh, 1993, "Experiment on melting in heat storage capsule with close contact and natural convection," Exp. Thermal Fluid Science, pp. 273-281.

[14] F.E.Moore, Y. Bayazitoglu, 1982, "Melting within a spherical enclosure," J. Heat Transfer, pp. 19-23.

[15] D. Nicholas, Y Bayazitoglu, 1980, "Heat transfer and melting front within a horizontal cylinder," J. Solar Energy, pp. 229.

[16] S.K. Roy, S. Sengupta, 1987, "Melting process within spherical enclosures," J. Heat Transfer, pp. 460-462.

[17] Rabinataj Darzi A A, Hassanzadeh Afrouzi H, Khaki M and Abbasi M., 2015, "Unconstrained melting and solidification inside rectangular enclosure," J. Applied Science, pp. 436-451.

[18] A.R. Archibold, J.G. Aguilar, M.M. Rahman, D.Y. Goswami, M. Romero, E.K. Stefanakos, 2014, " The melting process of storage materials with relatively high phase change temperatures in partially filled spherical shells," J. Applied Energy, pp. 243-252.

[19] Chorin, A. J., 1968, "Numerical solution of the Navier-Stokes equations," Mathematics of computation, 22(104), pp. 745-762.

[20] V.R. Voller, M. Cross, N.C. Markatos, 1987, "An enthalpy method for convection/diffusion phase change," Int. J. Numer. Meth. Eng, pp. 271-284.

[21] A.D. Brent, V.R. Voller, K.J. Reid, 1988, "Enthalpy porosity tecgnique for modeling convection diffusion phase change: application to the melting of a pure metal," Heat Transfer, pp.297-318.

[22] V.R Voller, 1996, "An overview of numerical methods for solving phase change problems," Advances in Numerical Heat Transfer, Chapter 9.

[23] V. Shatikian, G. Ziskind,R. Letan, 2005, "Numerical investigation of a PCM-based heat sink with internal fins," Int. J. Heat Mass Transfer, pp. 3689-3706.

[24] A.C. Kheirabadi, D. Groulx, 2015, "The Effect of the Mushy-Zone Constant on Simulated Phase Change Heat Transfer," Int. Sym. Advanced Computation Heat Transfer, pp. 460.

[25] L. Katsman, 2004, "Melting and solidification of a phase-change material (PCM)," Heat Transfer Laboratory, Department of Mechanical Engineering, Ben-Gurion University of the Negev.

[26] E. Assis, L. Katsman, G. Ziskind, R. Letan, 2004, "Experiment and numerical investigation of phase change in a spherical enclosure," Processdings of the fourth European Thermal Sciences Conference, Birmingham, UK.

VITA

Wen Xiong was born on November 22, 1991 in Wuhan, China, son of Jialiang Xiong and Hanjiao Qin. After finishing high school in 2011, he entered Huazhong University of Science and Technology and studied in the field of Mechanical Engineering in China. He completed the Bachelor of Science in Mechanical Engineering in 2015. After completing the B.S., he entered Lehigh University in 2015. He is currently a graduate student at Lehigh University.